Bioactive Materials 28 (2023) 255–272

Contents lists available at ScienceDirect

Bioactive Materials

journal homepage: www.keaipublishing.com/en/journals/bioactive-materials

O-alg-THAM/gel hydrogels functionalized with engineered microspheres based on mesenchymal stem cell secretion recruit endogenous stem cells for cartilage repair

Yucong Li [a,b,c,1], Linlong Li [a,b,c,1], Ming Wang [a,b,c], Boguang Yang [a,b,c], Baozhen Huang [a,b,c], Shanshan Bai [a,b,c], Xiaoting Zhang [a,b,c], Nan Hou [a,b,c], Haixing Wang [a,b,c], Zhengmeng Yang [a,b,c], Chong Tang [d], Ye Li [e], Wayne Yuk-Wai Lee [a,b], Lu Feng [a,b,c,**], Micky D. Tortorella [f,***], Gang Li [a,b,c,*]

[a] Stem Cells and Regenerative Medicine Laboratory, Li Ka Shing Institute of Health Sciences, The Chinese University of Hong Kong, Prince of Wales Hospital, Shatin, Hong Kong Special Administrative Region of China
[b] Musculoskeletal Research Laboratory, Department of Orthopaedics & Traumatology, Faculty of Medicine, The Chinese University of Hong Kong, Prince of Wales Hospital, Shatin, Hong Kong Special Administrative Region of China
[c] The CUHK-ACC Space Medicine Centre on Health Maintenance of Musculoskeletal System, The Chinese University of Hong Kong Shenzhen Research Institute, Shenzhen, PR China
[d] Department of Orthopaedics, Peking University Shougang Hospital, Beijing, PR China
[e] Department of Rehabilitation Sciences, Hong Kong Polytechnic University, Hong Kong Special Administrative Region of China
[f] Guangzhou Institutes of Biomedicine and Health, Chinese Academy of Sciences, Guangzhou, China

ARTICLE INFO

Keywords:
Bioactive hydrogels
Solidified secretome
Adhesive hydrogels
Acellular functional scaffold
Cartilage repair

ABSTRACT

Lacking self-repair abilities, injuries to articular cartilage can lead to cartilage degeneration and ultimately result in osteoarthritis. Tissue engineering based on functional bioactive scaffolds are emerging as promising approaches for articular cartilage regeneration and repair. Although the use of cell-laden scaffolds prior to implantation can regenerate and repair cartilage lesions to some extent, these approaches are still restricted by limited cell sources, excessive costs, risks of disease transmission and complex manufacturing practices. Acellular approaches through the recruitment of endogenous cells offer great promise for in situ articular cartilage regeneration. In this study, we propose an endogenous stem cell recruitment strategy for cartilage repair. Based on an injectable, adhesive and self-healable o-alg-THAM/gel hydrogel system as scaffolds and a biophysio-enhanced bioactive microspheres engineered based on hBMSCs secretion during chondrogenic differentiation as bioactive supplement, the as proposed functional material effectively and specifically recruit endogenous stem cells for cartilage repair, providing new insights into in situ articular cartilage regeneration.

1. Introduction

Articular cartilage is a unique connective tissue and functions to help the join movement by transmitting the movement-related loads. Lacking innate self-repair ability, small cartilage lesions may further progress to a serious joint degeneration and lead to osteoarthritis [1]. Stem-cell based therapy strategies are promising approaches for the treatment of cartilage defects. However, extensive cell expansion steps, the low rate

Peer review under responsibility of KeAi Communications Co., Ltd.

* Corresponding autho. Room 74038, 5F, Lui Chee Woo Clinical Science Building, The Chinese University of Hong Kong, Prince of Wales Hospital, Shatin, NT, Hong Kong Special Administrative Region of China.
** Corresponding autho. Room 501B, 5F, Li Ka Shing Medical Sciences Building, The Chinese University of Hong Kong, Prince of Wales Hospital, Shatin, NT, Hong Kong Special Administrative Region of China.
*** Corresponding author. Room A419, 4F, Building A, Guangzhou Institutes of Biomedicine and Health, Chinese Academy of Sciences, 190 Kai Yuan Avenue, Science Park, Guangzhou, 510530, China.
E-mail addresses: lufeng@link.cuhk.edu.hk (L. Feng), m.tortorella@gibh.ac.cn (M.D. Tortorella), gangli@cuhk.edu.hk (G. Li).
[1] These authors contributed equally to this work.

https://doi.org/10.1016/j.bioactmat.2023.05.003
Received 9 February 2023; Received in revised form 21 April 2023; Accepted 5 May 2023
Available online 31 May 2023

of cell survival and uncontrolled differentiation of stem cells transplanted into the body currently remain key challenges in advancing stem cell therapeutics. Therefore, activating, mobilizing, and recruiting endogenous stem cells represents an alternative strategy. Bone marrow stimulation technique, i.e., microfracture (MF), as the first-line and well-accepted treatment, is designed to recruit the endogenous mesenchymal stem cells (MSCs) from the bone marrow, which serve as an ideal autologous cell source for articular cartilage repair [2–4]. However, due to the inadequate capability of recruiting stem cells by MF and inefficient chondrogenic differentiation of recruited stem cells [5], long-term studies have shown that its clinical outcomes remain unsatisfactory [6], with scar formation and fibrocartilage filling defected cartilage. Therefore, functional and bioactive scaffolds with the abilities to recruit, program, and direct endogenous stem cells for cartilage repair represent a promising solution.

Most synthesized scaffolds currently used in cartilage repair such as hydrogels lack bioactive signals for cell attachment, growth, and differentiation [7]. The use of acellular products such as decellularized matrix and cell secretome for cartilage regeneration has gained popularity, due to the inherent compositional similarity and modulatory abilities of supporting tissue growth and differentiation [8]. These acellular products can effectively preserve bioactive proteins and regulatory growth factors while removing cellular components (DNA, lipids, etc.) that could lead to immunogenicity in vivo [9–11]. Furthermore, degradation products of decellularized matrix were reported to recruit endogenous stem and progenitor cells as chemoattractant and modulates innate immune response [12,13]. Previous studies have established that decellularized matrix from bone or cartilage was suitable for proliferation or chondrogenesis of MSCs, and successfully applied them in cartilage tissue engineering [14,15]. In comparison to tissue derived decellularized matrices, matrix and secretome derived from stem cell have specific functional and signaling capacity that cannot be readily reproduced [11,16,17]. The rich and complex set of molecules secreted from stem cells inherit abilities and functions from their origin cells, and mimic a microenvironment suitable for regeneration through physical interactions and paracrine signals. Therefore, in this study, we firstly engineered a type of bioactive microspheres based on hBMSCs secretion for endogenous stem cells recruitment and induction. Engineered microspheres were enriched with extracellular matrix (ECM) proteins and MSCs secretome, and therefore we named them microspheres of ECM and solidified secretome (MESS).

Although stem cell-based products including secretome, acellular matrix and exosome are potential game changers for the field of regenerative medicine. At the current stage of development, the shared challenge for the community is to scale up the quality of products and thereby safely translate them into applicable protocols [18,19]. As a safe, noninvasive biophysical strategy, pulsed electromagnetic fields (PEMF) have been extensively investigated and demonstrated to benefits stem cells including promoting proliferation and chondrogenic differentiation, increasing anabolic activities, and antagonizing the catabolic effects of inflammation [20–23]. In comparison to biochemical stimuli, biophysical cues such as PEMF could facilitate wider and more systemic effects on stem cells that universally enhance the quality of cells and cell products [24–26]. In our previous study, we have demonstrated that PEMF could promote the synthesize of chondrogenic ECM and prevent degenerative matrix production [27]. Therefore, Biophysio-stimulation with PEMF was utilized to enhance the quality and bioactivity of MESS.

As one of the most well-established scaffolds in cartilage repair, hydrogels are suitable to deliver the engineered MESS effectively and sufficiently into defected cartilage. Hydrogels made of various polymers have been shown to promote the chondrogenesis and cartilage regeneration in the presence of bioactive factors by providing the conducive 3D microenvironment [28,29]. Up to date, great success has been achieved in developing hydrogels for cartilage repair. However, it is still challenging to prepare hydrogels that can simultaneously fulfill the stringent requirements for real applications in cartilage tissue engineering. Such requirement usually includes excellent biocompatibility and bioactivity, desirable physical properties and mechanical performance, facile preparation, multiple application routes, etc. [30–32] Achieving a stable and appropriate integration with the target site for the injected hydrogel is a key factor in the treatment of cartilage defects. Without stable and adequate bonding towards the host tissue, fibrosis between the implanted hydrogels and host cartilage could easily occur, and the interfaces between the hydrogels and defect sites might easily disjoin, resulting in failure of the cartilage regeneration [33]. Because of the inherent adhesion ability to the target tissue, adhesive hydrogels could retain a stable situation in the injected area. Utilizing adhesive hydrogel in cartilage tissue engineering is a promising strategy to overcome the potential weak integration between biomaterials and host cartilage tissue. The dynamic Schiff-base bonds, formed by reactions between aldehyde and amino groups, with reversible breakage and re-formation features, not only enhance the mechanical properties of the hydrogel, but also endow the hydrogel with better injectability and self-healing properties [34]. Furthermore, hydrogels with aldehyde groups could effectively bind to the tissues through Schiff-base reaction, therefore granting them with tissue adhesive properties. Besides, adhesive hydrogels depending on hydrogen bonding for OA therapy have been prepared using polymers with plenty of hydroxyl groups [35–37]. Alginate, extracted from brown algae, has been widely used in biomedical engineering due to its biocompatibility and ease of gelation [38]. While original alginate hydrogels showed weak adhesion ability, so chemical modifications are needed to improve that property [39,40]. Modifying alginate through introducing aldehyde groups is designed to fabricate hydrogels with adhesive property. Gelatin is the hydrolysis product derived from collagen and is less immunogenic than collagen [41]. It is widely explored in tissue engineering because of its well-proven biocompatibility, biodegradability, low immunogenicity, and promotion on cell adhesion and proliferation [42]. Herein, by incorporating dynamic Schiff base covalent bonds and multiple hydrogen bonding, we propose a novel approach to prepare an injectable, self-healable, tissue adhesive and mechanically robust supramolecular hydrogel with oxidized alginate (o-alg), tris(hydroxymethyl) aminomethane (THAM) and gelatin.

Taken together, in this study we propose an endogenous stem cell recruitment strategy with a functional bioactive material consisting of o-alg-THAM/gel hydrogel system as scaffold and a hBMSCs-derived bioactive microspheres as bioactive supplement. The engineered microspheres, namely MESS, were fabricated based on hBMSCs secretion during chondrogenic differentiation, and enriched with ECM proteins and MSCs secretome. Biophysio-enhancement with pulsed electromagnetic field (PEMF) was also applied to elevate the quality and bioactivity of MESS. The PEMF enhanced MESS (PE-MESS) possess not only chondrogenic effects, but also facilitate stem cell recruitment, migration and aggregation and modulates cell inflammation response, which could potentially achieve comprehensive and balanced therapeutic effects during cartilage defect healing in the knee. From there, we further developed a functionalized o-alg-THAM/gel hydrogel system with desirable biocompatibility and injectable, self-healable and tissue adhesive properties, which harvested the biological functions of the PE-MESS and yet avoided its weaknesses such as weak mechanical properties. As we confirmed the therapeutic effects of our functionalized scaffold on chondrogenesis, stem cell migration and chemotaxis, and inflammation regulation through in vitro and in vivo testing, we believed that the as proposed functional material could effectively and specifically recruit endogenous stem cells for cartilage repair, revealing its therapeutic potential as a cell-free strategy in osteochondral defect healing in a rat model.

2. Results

2.1. Fabrication of o-alg/gel and o-alg-THAM/gel hydrogels

Oxidized alginate with different amounts of aldehyde groups was synthesized. Hydroxylamine hydrochloride method was conducted to determine the amounts of aldehyde groups of o-alg. As listed in Table S1, with the amounts of $NaIO_4$ and reaction time increasing, the amounts of aldehyde groups increased. In order to keep the amounts of residual aldehyde groups same for all the groups of o-alg and o-alg-THAM, o-alg with 0.00325, 0.0042, 0.00515 and 0.00635 mol/g aldehyde groups were selected and used furtherly.

The gelation mechanism of o-alg/gel and o-alg-THAM/gel hydrogels was that the Schiff base bonds would form after simply mixing the aldehyde groups-containing o-alg (o-alg-THAM) and amino groups-containing gelatin (Fig. 1. A). The introduction of THAM brings multiple hydrogen bonds into the hydrogel system, resulting in enhanced physical properties and mechanical strength.

As the main features of the injectable hydrogel system, gelation time and crosslinking degree were firstly studied for comparison. As shown in Table 1a, in all groups of o-alg/gel hydrogels, under the same concentration of o-alg, the gelation time of the hydrogel was gradually decreased with the oxidation degree of o-alg increasing, ranging from 11 min to 5 min. After introducing THAM onto o-alg, as shown in Table 1b, under the same amounts of aldehyde groups with the amounts of THAM increasing, the gelation time of the hydrogel was slightly increased, ranging from 11 min to 13 min. This may be attributed to the hydrogen bonding that may hinder the reaction of aldehyde groups with amino groups.

As listed in Table 1b, different groups of o-alg-THAM/gel hydrogels exhibited almost the same crosslinking degree. Through selection of o-alg raw materials with different amounts of aldehyde groups, after grafting relevant amounts of THAM, the residual amounts of aldehyde groups were nearly the same. Thus, for different groups of hydrogels, the

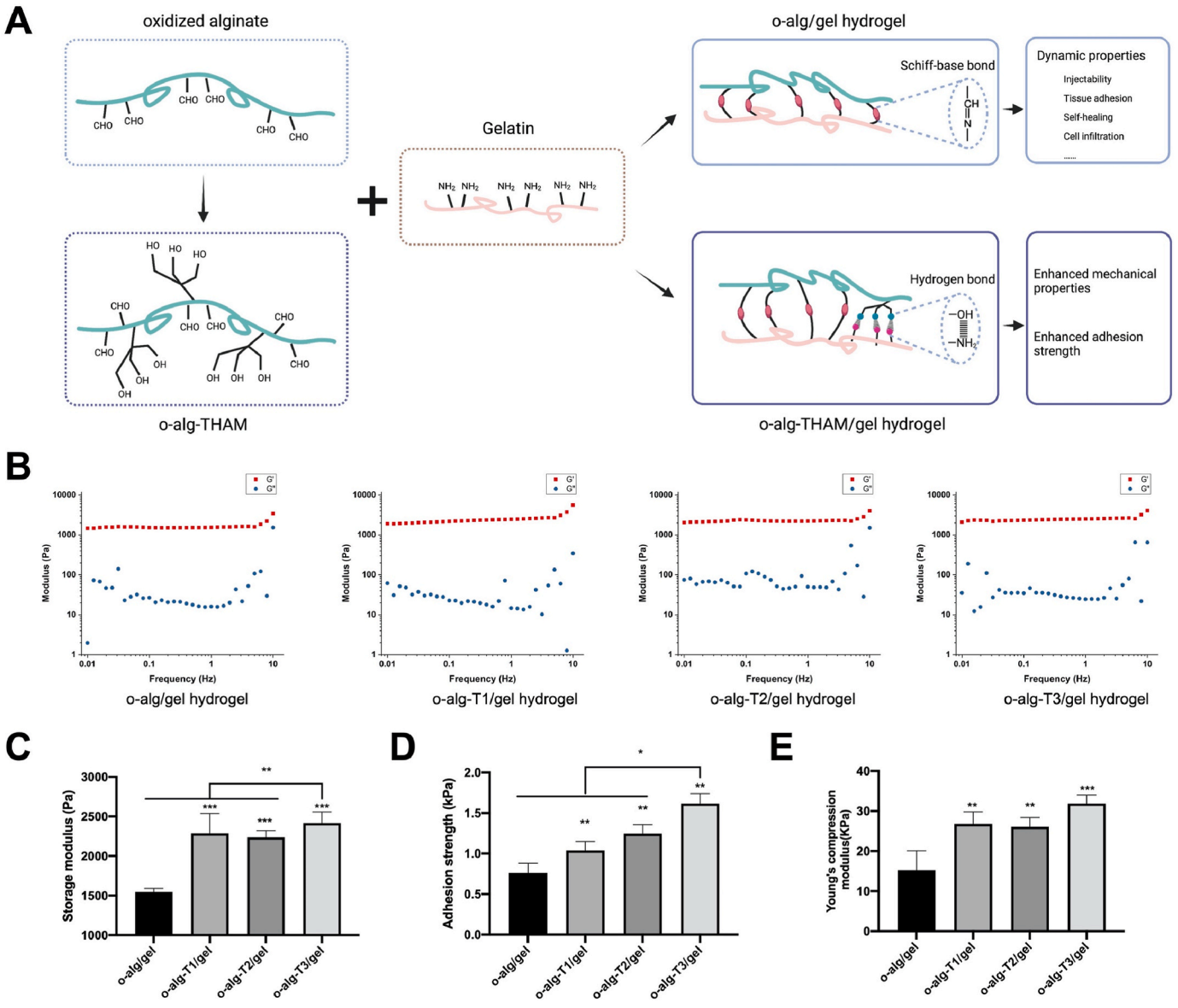

Fig. 1. Fabrication and characterization of o-alg/gel and o-alg-THAM/gel hydrogels. **A** Schematic illustration of the crosslinking mechanisms of o-alg/gel and o-alg-THAM/gel hydrogels. (Created with BioRender.com) B Frequency dependence of storage modulus (G′) and loss modulus (G″) of o-alg/gel, o-alg-T1/gel, o-alg-T2/gel and o-alg-T3/gel hydrogels. **C** Comparison of average storage modulus based on frequency sweep (n = 4/group). **D** Adhesion properties of o-alg/gel, o-alg-T1/gel, o-alg-T2/gel and o-alg-T3/gel hydrogels through lap-shear adhesion test (n = 5/group). **E** Young's compression modulus of o-alg/gel, o-alg-T1/gel, o-alg-T2/gel and o-alg-T3/gel hydrogels (n = 4/group). *p < 0.05, **p < 0.01, ***p < 0.001.

Table 1
Group information of different o-alg/gel hydrogels and o-alg-THAM/gel hydrogels and their gelation time and crosslinking degree.

Samples	m (o-alg)	m (THAM)	Gelation time	Crosslinking degree
a				
o-alg-1/gel	0.04 g (0.00020 mol)	-	11 min	-
o-alg-2/gel	0.04 g (0.00020 mol)	-	9 min	-
o-alg-3/gel	0.04 g (0.00020 mol)	-	6 min	-
o-alg-4/gel	0.04 g (0.00020 mol)	-	5 min	-
b				
o-alg-1/gel (o-alg/gel)	0.04 g (0.00020 mol)	0	11 min	43.58 ± 2.81%
o-alg-2-THAM/gel (o-alg-T1/gel)	0.04 g (0.00020 mol)	0.0048 g (0.00004 mol)	12 min	43.48 ± 3.14%
o-alg-3-THAM/gel (o-alg-T2/gel)	0.04 g (0.00020 mol)	0.0097 g (0.00008 mol)	12 min	42.77 ± 3.88%
o-alg-4-THAM/gel (o-alg-T3/gel)	0.04 g (0.00020 mol)	0.0145 g (0.00012 mol)	13 min	44.55 ± 3.04%

crosslinking degrees were similar.

We next compared the physical properties of o-alg/gel and o-alg-THAM/gel hydrogels. The frequency sweep of 0.01 Hz–10 Hz was used to measure the variations of storage modulus (G′) and loss modulus (G″) with the frequency. As shown in Fig. 1. B, for all the samples, the G′ was distinctly higher than G" in the whole tested frequency range. In addition, the G′ remained stable among the whole frequency range, showing approximately a frequency-independent characteristic. In comparison with o-alg/gel hydrogels, the G′ significantly increased in all three groups of o-alg-THAM/gel hydrogels. With the amounts of THAM increased, the G' increased as well (Fig. 1. C).

The adhesive strength of injectable hydrogel to moist tissue is a key factor for cartilage defect filling. Therefore, lap-shear stress test was carried out by placing hydrogels between two gelatin-covered glass slides. For the o-alg/gel group, without additional THAM, hydrogels showed relative lower adhesion strength than the o-alg-T/gel hydrogel groups. This could indicate that through introducing multiple hydrogen bonding, the adhesion ability of the composite hydrogel could be effectively promoted. As shown in Fig. 1. D, after the introduction of THAM, the o-alg-THAM/gel hydrogels displayed improved adhesion abilities compared with the o-alg/gel hydrogels. Results showed that o-alg-T3/gel hydrogels showed the adhesion strength of 1.618 ± 0.122 kPa, which was significantly higher than other groups of hydrogels. The mechanical property was also enhanced by the introduction of THAM. Significantly increased Young's compression modulus in the o-alg-THAM/gel hydrogels was observed compared with the o-alg/gel hydrogels (Fig. 1. E).

Based on the above results, o-alg-T3/gel hydrogels were selected and

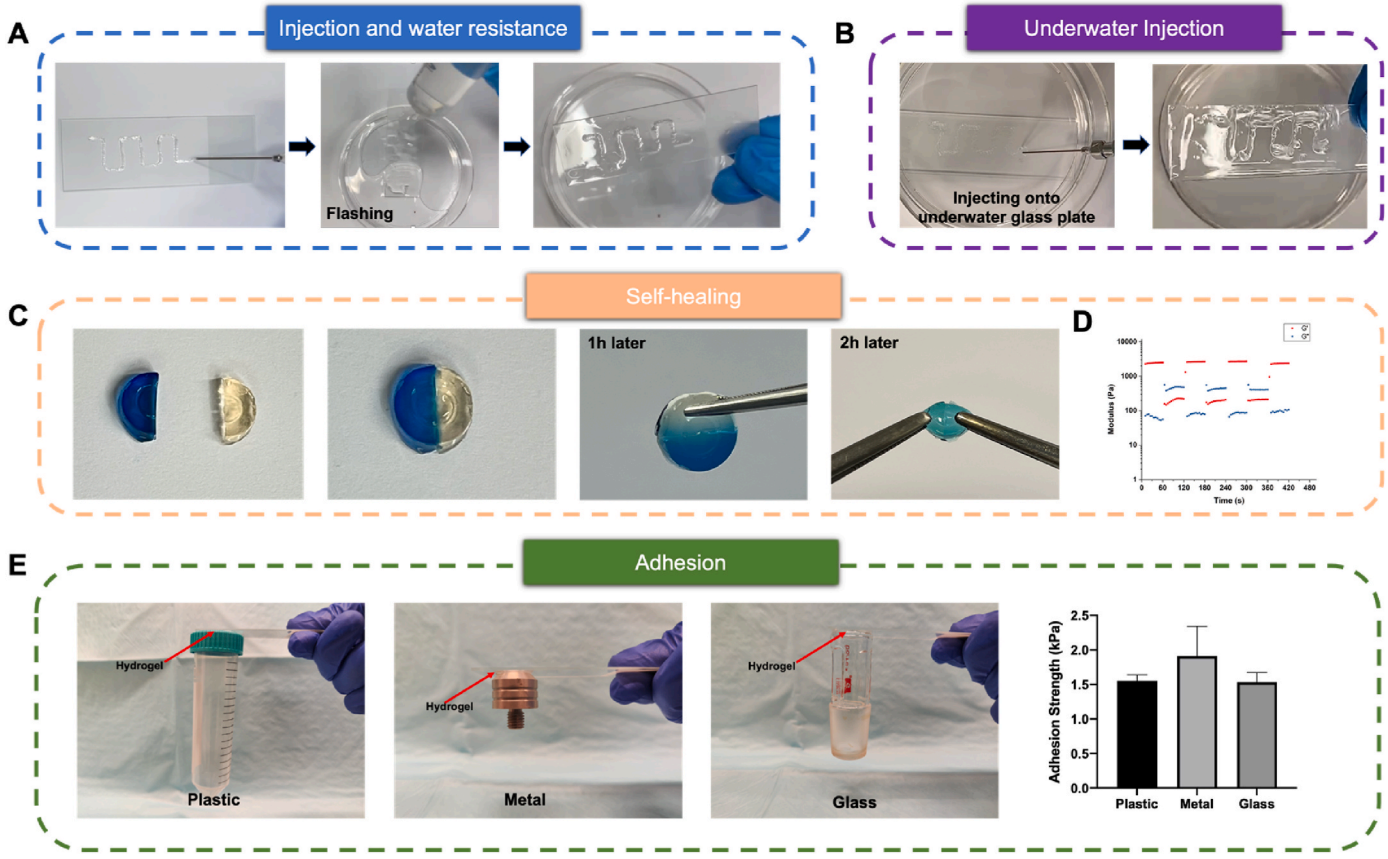

Fig. 2. Physical properties of o-alg-THAM/gel hydrogels. A Illustration of the injectability and adhesiveness of o-alg-THAM/gel hydrogels. Hydrogels could firmly adhere onto the glass slide under constant flow of water. **B** Illustration of injecting o-alg-THAM/gel hydrogel onto an underwater glass slide. Hydrogel in situ formed and adhered on the underwater glass slide. **C** llustration of the self-healing ability of o-alg-THAM/gel hydrogels. **D** The time sweep test with cyclic strain on o-alg-THAM/gel hydrogels. E Adhesiveness of o-alg-THAM/gel hydrogels on various substrates, such as plastic, metal, and glass. Adhesion stress of o-alg-THAM/gel hydrogels on various substrates were tested at 37 °C (n = 3).

used for the following biological validation studies.

2.2. Injectability, adhesiveness and self-healing ability of o-alg-THAM/gel hydrogels

The o-alg-THAM/gel hydrogels showed desirable injectability, adhesiveness and self-healing ability. As shown in Video 1 and Fig. 2. A, the prepared hydrogel could be injected smoothly from a 23G needle and then rapidly and firmly attached to the gelatin-covered glass slide. Even under constant flow of water, the hydrogel could still firmly adhere onto the glass slide. Furthermore, an underwater injection and adhesion test was also conducted and shown in Fig. 2. B and Video 2. The as-prepared hydrogel could be injected smoothly and attached onto the gelatin-coated glass slide underwater. This could indicate that during surgical procedure, under body fluid or effusion of blood, the injected hydrogel could still effectively adhere to the defect sites. The adhesiveness of o-alg-THAM/gel hydrogels were tested on various substrates, such as plastic, metal, and glass (Fig. 2. E). As demonstrated, hydrogel could tightly adhere onto the surface of these substrates without detachment.

Supplementary video related to this article can be found at https://doi.org/10.1016/j.bioactmat.2023.05.003

The self-healing ability of o-alg-THAM/gel hydrogel was demonstrated in Fig. 2. C. The two half pieces of the original and stained hydrogel were brought into contact at 37 °C under moist conditions. After 1 h, the cut hydrogel pieces would gradually self-heal into an integrated hydrogel after contacting with each other. And the hydrogel could also be stretched to the opposite direction after 2 h of self-healing process. The time sweep with cyclic strain was further conducted to illustrate the self-healing property of the hydrogels. As shown in Fig. 2. D, G′ was obviously higher than G″ under 1% strain. When the strain increased to 100%, G′ sharply decreased and was lower than G”. When the applied strain was reduced to 1%, G’ was recovered and was higher than G” again.

2.3. Engineering microspheres of ECM and solidified secretome (MESS) from hBMSCs aggregates

2.3.1. Engineering and characterization of MESS

In our study, MESS were successfully engineered by decellularization of chondrogenic induced hBMSCs aggregates (Fig. 3A). The amount of cells per hBMSCs aggregates were settled as 20,000, determined according to the decellularization efficacy and sGAG content preservation ratio (Supplementary Fig. S1). Scanning electron microscopy (SEM) was used to characterize the morphology and size distribution of the engineered MESS (Fig. 3 B). As demonstrated, the MESS in spherical shape with a rough and porous surface. The shape and structure of MESS were not disrupted by the decellularization. The mean diameter of MESS was measured as 199.7 ± 48.6 μm.

2.3.2. Proteomics analysis revealed the enriched secreted proteins in MESS

By iTRAQ-based proteomics, analysis on three biologically independent replicates of MESS and PE-MESS identified 380 secreted human protein components (Fig. 3. D). Of these, 255 could be identified as vesicle proteins, including 174 extracellular vesicle (EV) proteins, and 87 could be identified as ECM proteins, including collagen, fibronectin, glycoproteins, proteoglycans. 11 growth factors including TGF-β1, TGF-β3, CTGF, and FGF1 were identified. SDF-1, the key chemokine in MSCs was also identified, indicating the potential function of MESS in endogenous MSCs recruitment. The Gene Ontology (GO) enrichment suggested that secreted proteins identified in MESS were enriched in biological processes including cell adhesion, inflammatory response, and differentiation. KEGG enrichment and protein-pathway interactions were performed to further investigate the biological functions of the secreted proteins in MESS (Fig. 3. E and F). Enriched proteins were implicated in focal adhesions and ECM-receptor interactions, potentially facilitating ECM-cell interactions.

2.3.3. Enhancing the quality of MESS with pulsed electromagnetic fields (PEMF)

PEMF stimulation was applied during the chondrogenic induction of hBMSCs aggregates into micromasses. Our previous study has demonstrated that PEMF stimulation with an FDA approved signal could promote BMSCs chondrogenic differentiation and mitigate cell hypertrophy process [27]. In this study, we also confirmed that daily PEMF stimulation could effectively promote the chondrogenic differentiation of hBMSCs during micromass culture (Supplementary Fig. S2). By a thorough investigation on hBMSCs from three donors, we found that daily PEMF stimulation could consistently and significantly promote the expression of chondrogenic genes (Sox9, ACAN and Col2a1) and matrix protein collagen type II, and inhibit the expression of hypertrophic genes and degeneration matrix protein collagen type X.

Based on these findings, we enhanced the quality of MESS with PEMF stimulation. In comparison with MESS, the PEMF enhanced MESS (PE-MESS) were found to contain more SDF-1, chondrogenic growth factors including TGF-β1 and TGF-β3, and matrix proteins including collagen and fibronectin (Supplementary Fig. S3). These findings indicated that PE-MESS may potentially present more superior biological functions than MESS.

2.4. Fabrication of MESS hydrogels and PE-MESS hydrogels

O-Alg-THAM solution and gelatin solution were prepared as described above. Engineered MESS and PE-MESS were firstly suspended evenly in gelatin solution (20 mg MESS/PE-MESS in 1 mL gelatin solution) and then mixed with o-Alg-THAM solution to initiate gelation (Fig. 4. A). The self-gelling process based on Schiff reaction initiated immediately after mixing, and the aldehyde groups would react with amine groups in gelatin as well as MESS, crosslinking MESS into the hydrogel network. Protein release profiles from MESS embedded in o-Alg-THAM/Gel hydrogels, demonstrated sustained-release kinetics into the supernatant. In contrast, soluble protein products such as BSA supplemented into hydrogels showed a burst release profile (Fig. 4. C). The sustained release of proteins and cytokines from MESS and PE-MESS would create chemoattractant gradients surrounding microspheres, inducing recruitment of cells to form aggregates, and then in time functionalize the entire hydrogel with bioactive molecules, creating a suitable microenvironment for chondrogenesis (Fig. 4. B). The release of SDF-1, the key chemokine in stem cell chemotaxis, was also studied (Fig. 4. C). The sustained release of SDF-1 was observed in both MESS and PE-MESS hydrogels. Significantly more SDF-1 was released from PE-MESS compared to MESS.

2.5. Functionalized hydrogels facilitated MSCs migration and chondrogenic differentiation and presented anti-inflammatory effects on macrophages in vitro

To demonstrate the functionalized hydrogels can potentially facilitate cell infiltration and migration, we seeded GFP-MSCs on the surface of hydrogels and allow the cells to migrate for 12hrs. As shown in Fig. 4. D, after 12 h of culture, very few MSCs infiltrated into the blank hydrogel. In MESS hydrogels, more cells infiltrated, yet most of which still remained on top of the hydrogels, whereas in PE-MESS hydrogels much more MSCs infiltrated and migrated much deeper into the hydrogels and interactions between cells and microspheres can be observed. Quantitative analysis confirmed that significantly more MSCs infiltrated inside PE-MESS hydrogels hydrogels in comparison with Blank and MESS hydrogels (Fig. 4. E). In comparison with Blank hydrogel group, MESS hydrogels also demonstrated a significant effect on facilitating MSCs migration, with significantly more cells infiltrated inside the hydrogels. Infiltration depth of MSCs in PE-MESS hydrogels was also significantly deeper than that in blank and MESS hydrogels.

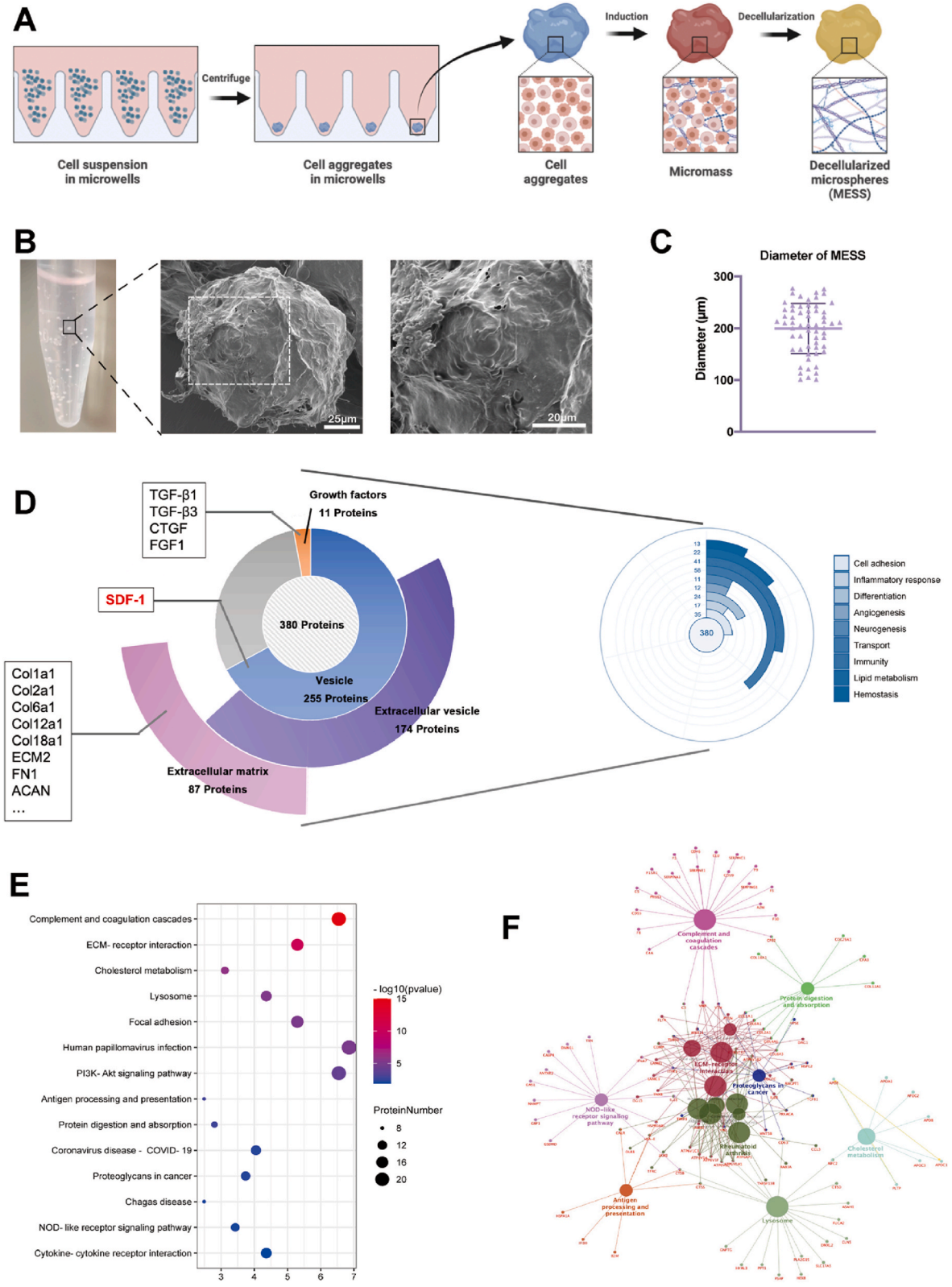

Fig. 3. **A** Schematic illustration of the flow of engineering MESS (Created with BioRender.com). **B** Macroscopic appearance and scanning electron microscopic images of MESS. **C** Diameter of MESS measured from SEM images. **D** Secreted protein components in MESS identified with proteomics analysis. Pie diagrams visualizing the role of identified secretome proteins from three biological replicates classified by GO CC (left diagram), and their biological functions enriched in GO BP (right diagram). **E** Top enriched pathways of secreted proteins in MESS using KEGG database in DAVID bioinformatics, organized by pvalue as well as protein counts. **F** Protein-pathway interactions visualized Layout using ClueGo in Cytoscape.

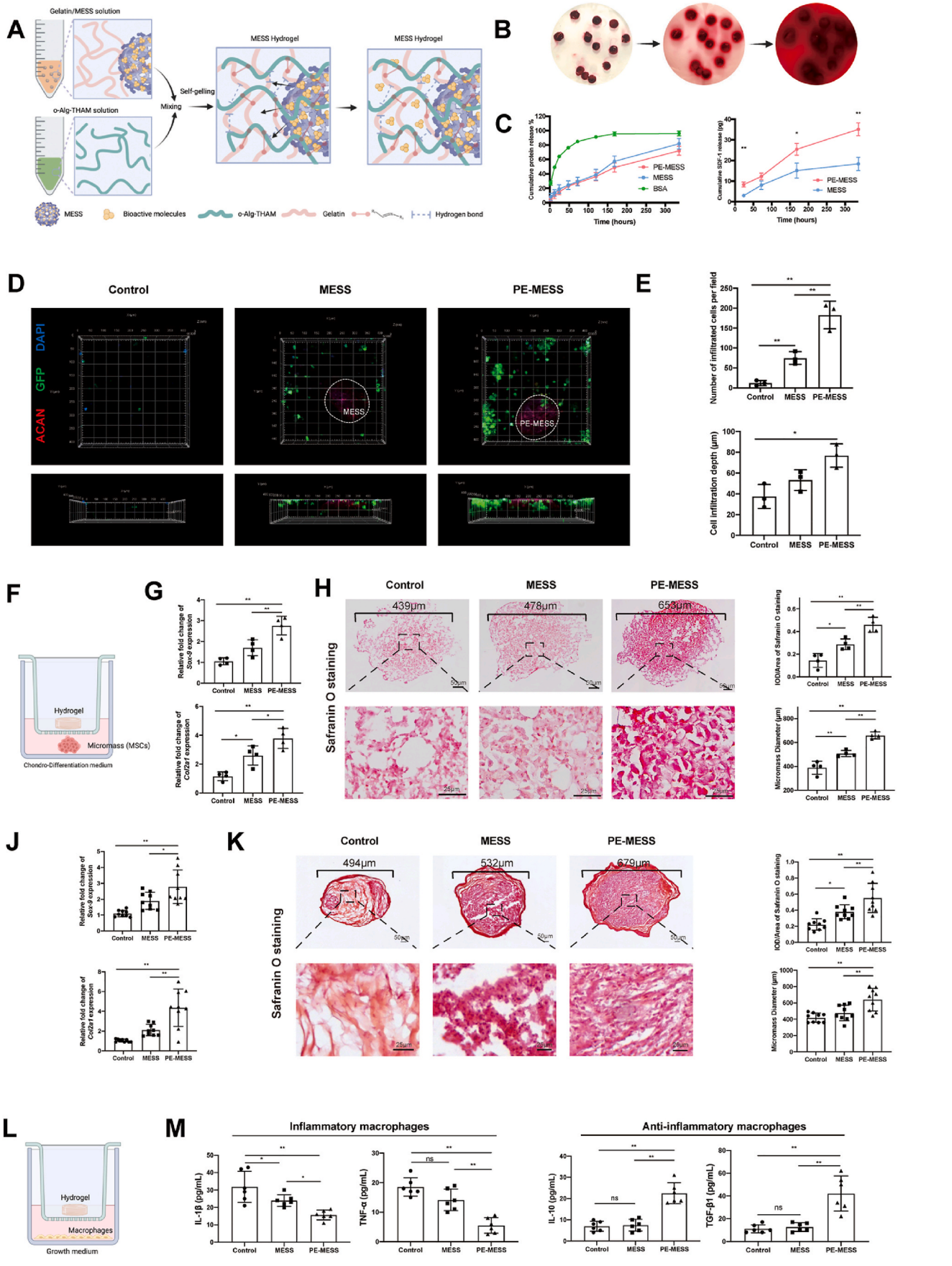

(caption on next page)

Fig. 4. **A** Schematic illustration of MESS and PE-MESS hydrogel preparation (*Created with* BioRender.com). **B** Illustration of bioactive molecule gradients in hydrogels created by MESS. **C** Cumulative protein release profiles of BSA, MESS and PE-MESS in hydrogels estimated using BCA assay (Left diagram) and cumulative SDF-1 release of MESS and PE-MESS in hydrogels estimated by ELISA (Right diagram). **D** Confocal images of rat GFP-MSCs migration assay in blank hydrogel, MESS hydrogel and PE-MESS hydrogel in vitro. **E** Statistical quantitative analysis of confocal scanning images. **F–H** The chondro-inductive effects of MESS and PE-MESS hydrogels were investigated on rMSCs micromasses using a transwell system. qPCR (**G**) and safranin O staining with statistical quantitative analysis (**H**) were performed. n = 4/group. **J-K** The chondro-inductive effects of MESS and PE-MESS hydrogels were investigated on hBMSCs micromasses using a transwell system. hBMSCs from 3 different donors were used. qPCR (**J**) and safranin O staining with statistical quantitative analysis (**K**) were performed. n = 3/donor/group. **L-M** The regulative effects of MESS and PE-MESS hydrogels on macrophages were investigated using a transwell system. ELISA analysis of IL-1β, TNF-α, IL-10 and TGF-β1 were performed. n = 6/group. *p < 0.05, **p < 0.01.

The chondrogenesis effects of the functionalized hydrogels were investigated in both rBMSCs and hBMSCs by transwell assay. As demonstrated in Fig. 4 F–I, MESS hydrogels and PE-MESS hydrogels can significantly promote the expression of chondrogenic genes Sox-9 and collagen II in rBMSCs after 14 days of micromass culture, comparing with control. PE-MESS hydrogels showed significantly stronger promoting effects on the expression of chondrogenic genes compared with MESS hydrogels. Safranin O staining also demonstrated that MESS hydrogels and PE-MESS hydrogels can significantly promote chondrogenic matrix formation. In comparison with MESS hydrogels, PE-MESS hydrogels showed significantly greater chondroinductive effects. In PE-MESS group, formation of chondrogenic matrix were significantly increased in micromasses with significantly larger diameter. Similar chondroinductive effects of MESS hydrogels and PE-MESS hydrogels were also observed on hBMSCs. PE-MESS hydrogels showed significantly greater chondroinductive effects compared with blank and MESS hydrogels, by promoting the expression of chondrogenic genes and formation of chondrogenic matrix in micromass culture.

The anti-inflammatory effects of the functionalized hydrogels were investigated on rat inflammatory and anti-inflammatory phenotypes of macrophages using a transwell system. ELISA tests on the conditioned medium indicated that PE-MESS could significantly downregulate the secretion of inflammatory factors IL-1β and TNF-α in inflammatory macrophages, and upregulate the secretion of anti-inflammatory factors IL-10 and TGF-β1 in anti-inflammatory macrophages, indicating the best anti-inflammatory effects among all types of hydrogels. MESS demonstrated inhibiting effects on the secretion of IL-1β and TNF-α in M1 macrophages, but no effects on M2 macrophages compared to control. Through this experiment, we have primarily revealed the anti-inflammatory effects of MESS and PE-MESS hydrogels in rat macrophages. However, in order to get more convincing evidence to facilitate clinical translation, future studies are still needed to further confirm these effects on human macrophages and other immune cells.

2.6. Bioactive properties of MESS and PE-MESS hydrogels in vivo

2.6.1. Functionalized hydrogels present good biocompatibility in vivo

Rat subcutaneous implantation was performed to investigate the biocompatibility and biological effects of the hydrogels in vivo (Fig. 5. A). The macroscopic examination of the hydrogels after 14 days implantation was shown in Fig. 5. B. No obvious inflammation was observed surrounding either type of the hydrogels, and healthy tissue could be observed surrounding the hydrogels with the presence of an enriched vascular network. The global view of H&E staining (Fig. 5. C) showed that no sign of acute inflammation was observed in the surrounding tissues of all hydrogels, indicating their good biocompatibility.

2.6.2. PE-MESS hydrogels present stem cell chemotaxis and immunoregulation effects in vivo

H&E staining results (Fig. 5. C) demonstrated the effects of functionalized hydrogels on cell chemotaxis. After 14 days of implantation, only a small number of cells infiltrated into the blank hydrogels, and most of the cells gathered in regions near the border to surrounding tissue. Much more cells were observed to infiltrate inside the MESS hydrogels and PE-MESS hydrogels. A large number of cells were observed to migrate into the center of the hydrogels. Cells migrated towards and aggregated surrounding the MESS, and evenly distributed in the rest regions of the hydrogels. IF staining was performed to further identify the type of cells migrated inside hydrogels. Our results indicated that in either type of the hydrogels, significantly less $CD68^+$ cells (macrophages) and CD11b + cells (neutrophils) were found compared to healthy skin tissue, indicating that o-alg-THAM/Gel hydrogels present good biocompatibility in vivo and cause no inflammatory response. In PE-MESS hydrogels, a significant decrease of macrophage and neutrophil numbers was observed in comparison of the other types of hydrogels, indicating that PE-MESS could provide anti-inflammation effects via regulating immune cells. A significant decrease of neutrophils was also observed in MESS hydrogels in comparison with blank hydrogels, which was not observed in macrophages. This indicates that MESS hydrogels also provide anti-inflammation effects, which is not as strong as PE-MESS hydrogels. The number of MSCs migrated inside were also observed to increase in MESS and PE-MESS hydrogels. PE-MESS hydrogels demonstrated better MSCs recruitment abilities compared with other hydrogels. Significantly more MSCs were observed to be recruited inside MESS hydrogels compared with blank hydrogels, demonstrating desirable stem cells chemotaxis effects of engineered MESS. Moreover, significantly more MSCs were attracted and migrated inside PE-MESS hydrogels in comparison with both blank and MESS hydrogels, and a large number of MSCs gathered surrounding PE-MESS, indicating that PE-MESS can provide stem cells chemotaxis effects and facilitate stem cell aggregation surrounding the microspheres.

2.7. Functionalized hydrogels promote the regeneration of cartilage and subchondral bone in the rat osteochondral defect model

We further assess the efficacy of our functionalized hydrogels as a cell-free strategy for cartilage and subchondral bone regeneration in the osteochondral defect in rat knee. Decellularized cartilage matrix microparticles (tECM) loading hydrogels were used as positive control as its a well-established and widely reported strategy [43–46]. 4 weeks after surgery, as shown in Fig. 6. B, histological examination using Safranin-O & Fast Green staining revealed the deposition of disorganized fibrous tissue on the surface of the osteochondral defects and limited regeneration of subchondral bone in the non-treatment negative control (NC) group. In blank hydrogel group, large amount of hydrogel residuals remained inside the defect site, with fibrous tissue covered on top and limited subchondral bone regeneration. The implanted hydrogels were tightly surrounded by newly regenerated tissues and regenerated subchondral bone were observed to infiltrate inside the hydrogels, indicating their good biocompatibility. In tECM and MESS groups, regeneration of subchondral bone was remarkably enhanced compared to NC and blank hydrogel groups. However, in tECM group, still disorganized fibrous tissue was observed covering the surface of the defect, whereas an enhanced chondrogenesis activity was observed near the surface of the defect on top of the regenerated subchondral bone in MESS group. In comparison with other 4 groups, a clear enhancement of the regeneration of cartilage and subchondral bone was observed in PE-MESS group. The articular surface was covered by cartilage-like tissue with smooth integration to the surrounding tissue, and large scale of cell aggregation and chondrogenic matrix deposition was observed. The subchondral bone was almost fully regenerated, and the residual hydrogels were surrounded by newly regenerated bone. 8

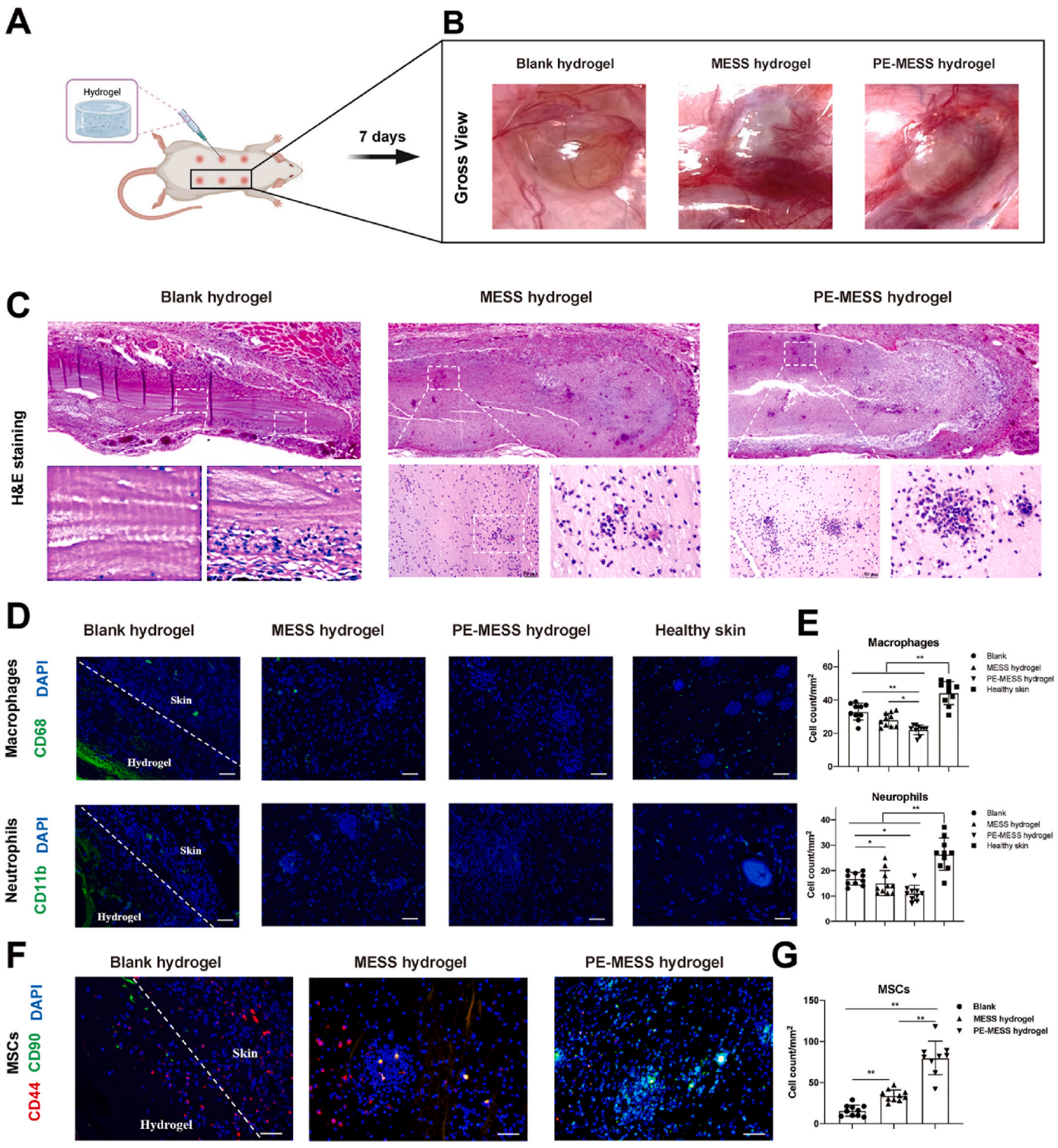

Fig. 5. **A** Illustration of subcutaneous implantation of hydrogels by on the back of rats by injection. B Gross view of hydrogels 7 days after implantation. C H&E staining of hydrogels 7 days after implantation. D-E IF staining of CD68 and CD11b and semi-quantitative analysis. F-G Double labeling IF staining of CD44 and CD90 and semi-quantitative analysis of CD44 and CD90 double-positive cells recruited into the hydrogels. *p < 0.05, **p < 0.01.

weeks after surgery, the osteochondral defect in NC group was poorly healed, with disorganized fibrous tissue on the surface and little regenerated subchondral bone inside. In blank and tECM hydrogel groups, better subchondral bone regeneration was achieved, whereas the articular surface was still covered with fibrous tissue with poor integration with native cartilage. In MESS hydrogel group, the defect was filled with a mixture of fibrous and cartilage-like tissue with enhanced regeneration of the subchondral bone. In clear contrast, the defects in the PE-MESS hydrogel group show more congruent articular surface and enhanced regeneration of hyaline cartilage with similar articular cartilage structure. Restoration of subchondral bone with organized structure was also observed. IHC staining of Col II (Fig. 6. C and E) confirmed the findings from histology staining. Significantly more cartilaginous matrix was observed in MESS hydrogel and PE-MESS hydrogel groups at both 4 and

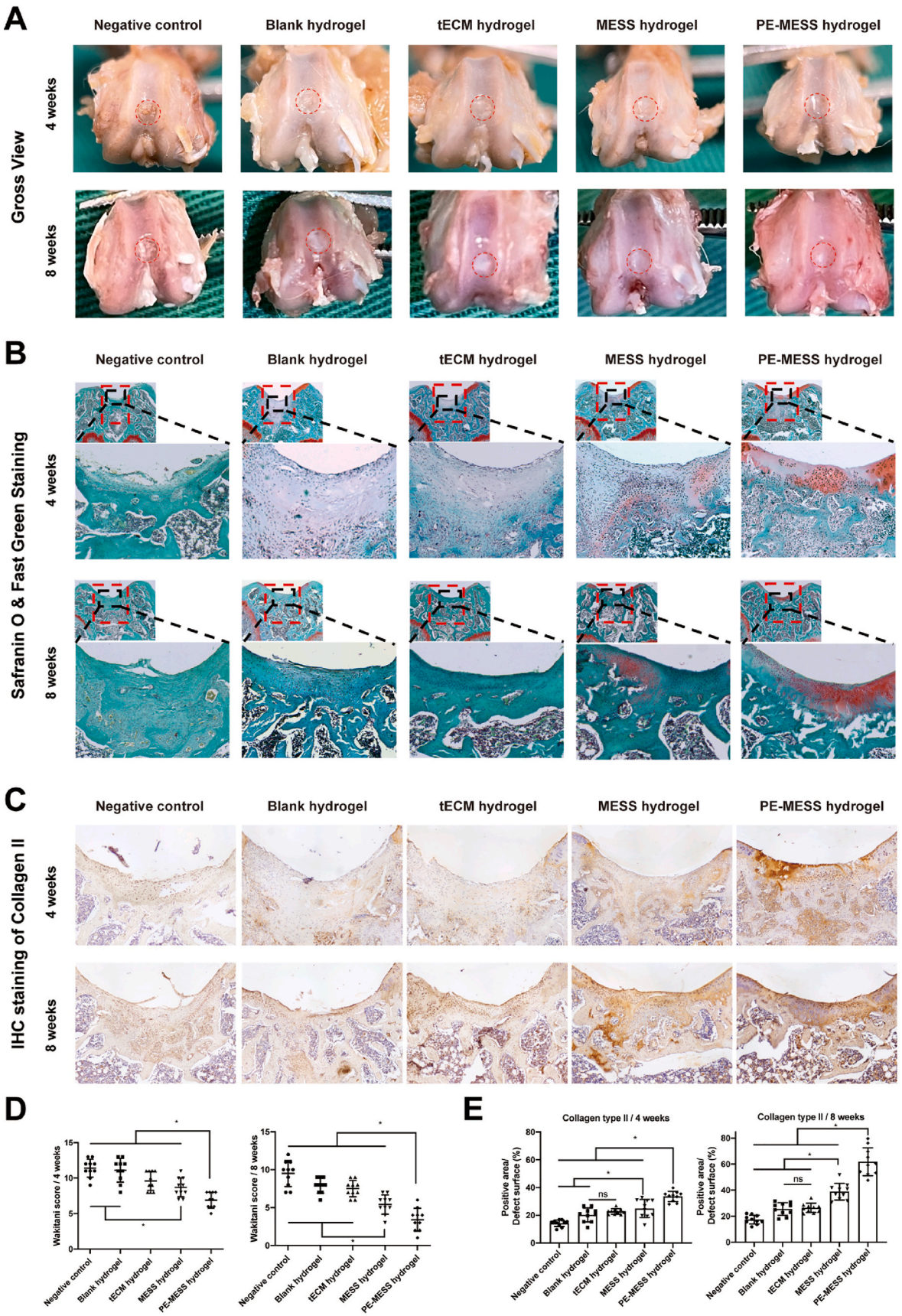

Fig. 6. **A** Macroscopic appearance of the rat osteochondral defect. **B** Safranin O & Fast Green staining of the rat osteochondral defect sections. C Immunohistochemical staining of type II collagen. D Cartilage regeneration evaluated by the Wakitani scoring system E Semi-quantitative analysis of IHC staining of collagen type II. *p < 0.05, ns: no significance, n = 10/group/time point.

8 weeks in comparison with NC, blank hydrogel and tECM hydrogel groups, indicating that the composite functional scaffolds present desirable therapeutic effects in cartilage defect repair. In comparison with MESS hydrogel group, PE-MESS hydrogel showed significantly stronger promoting effect on cartilaginous matrix deposition, and revealed superior therapeutic potential. The quality of the cartilage regeneration is evaluated according to Wakitani scoring system [47] (Fig. 6. D). At 4 and 8 weeks, PE-MESS hydrogel achieved lowest score, demonstrating the best healing outcomes of osteochondral defect. Rats from MESS hydrogel group were scored significantly lower than NC, blank hydrogel and tECM hydrogel groups, indicating that MESS hydrogel also provide beneficial effects for cartilage and subchondral bone repair, although inferior to PE-MESS hydrogels. However, in comparison with blank hydrogel group, tECM hydrogels didn't reveal significant positive effects on cartilage repair in terms of promoting chondrogenic matrix deposition or enhancing cartilage regeneration quality evaluated by Wakitani score. This indicates that in the proposed strategy of endogenous MSCs recruitment for cartilage repair, tissue derived dECM might not be suitable as bioactive supplement microparticles, probably because of insufficient bioactivities due to lacking relevant growth factors and chemokines.

3. Discussion

In our processing approach, we fabricated a type of biophysio-enhanced hBMSCs-derived PE-MESS as functional supplement, and an injectable, self-healable, tissue adhesive and mechanically robust supramolecular hydrogel, o-alg-THAM/gel hydrogels as scaffold. Thereby, a functionalized scaffold system was successfully engineered as a cell-free strategy for osteochondral defect tissue engineering. The design of this functional material is to use the sustained protein release of PE-MESS to create a chemoattractant gradient to recruit endogenous cells, especially stem cells into the hydrogels and towards PE-MESS. Meanwhile, the chondrogenic matrix of PE-MESS enriched with multiple growth factors creates microenvironment suitable for stem cell colonization, aggregation and chondrogenic differentiation.

An increasing body of evidence indicates that MSCs exert their therapeutic effects largely through their paracrine actions [48], and it has been hypothesized that proteins and signaling cytokines secreted by MSCs tend to induce surrounding cells into the same biological process. Therefore, MESS was designed and engineered with the purpose of facilitating endogenous MSCs recruitment and chondrogenesis based on hBMSCs secretion during chondrogenic differentiation. The engineered MESS were shown to consist various growth factors, cytokines, chemokines and extracellular matrix components, and present desirable biological functions. PEMF was also utilized to enhance the quality of MESS due to its effects on promoting MSCs secretion. In this study, we performed in vitro and in vivo studies to evaluate the bioactivities of engineered MESS and PE-MESS, and explored their therapeutic potential in cartilage repair. Our results demonstrated that the obtained MESS and PE-MESS could effectively facilitate stem cell migration and recruitment, induce recruited MSCs towards chondrogenic differentiation, and provide anti-inflammatory effects. In comparison with MESS, the above-mentioned bioactivities were all enhanced in PE-MESS, indicating that by promoting hBMSCs chondrogenesis and cell serection, PEMF stimulation effectively improved the quality of MESS, which may contribute to clinical translation and mass production of MESS in the future.

To facilitate endogenous stem cell recruitment, it is also essential to create chemoattractant gradients in the injury site of the cartilage. Therefore, we suspended the engineered MESS evenly inside the hydrogels. Our in vitro study demonstrated that the natural structure and insoluble natural of MESS grant them sustained-release kinetics, which would create chemoattractant gradients surrounding MESS. These are the advantages that cannot be achieved by traditional stem cell secretome, which is soluble and would demonstrate a burst release profile when loaded into hydrogels.

Due to the inherent compositional similarity and modulatory abilities of supporting tissue growth and differentiation, the use of acellular products such as decellularized matrix and cell secretome for cartilage regeneration has gained popularity [8]. Stem cell derived matrix and secretome have potential to guide cell differentiation into appropriate tissue types and supports in vivo tissue remodeling and regeneration [49,50]. Furthermore, degradation products of decellularized matrix were reported to recruit endogenous stem and progenitor cells as chemoattractant and modulates innate immune response [12,13]. Previous studies have applied decellularized matrix particles from bone or cartilage in cartilage tissue engineering, and achieved positive outcomes. Meng et al. fabricated a composite scaffold with demineralized bone matrix particles and chitosan hydrogel, which promoted proliferation and chondrogenesis of rat BMSC and was suitable for cartilage tissue engineering [14]. Lu et al. combined the oriented ACM scaffold with the RAD/PFS hydrogel for cartilage engineering by mending the microenvironment of the defect for cartilage regeneration [5]. However, in this study, cartilage derived dECM particles (tECM) was used as positive control and evaluated through in vivo study with rat osteochondral defect model. However, tECM hydrogels didn't reveal significant positive effects on cartilage repair. This indicates that in the proposed strategy of endogenous MSCs recruitment for cartilage repair, tissue derived dECM might not be suitable as bioactive supplement microparticles, probably because of insufficient bioactivities due to lacking relevant growth factors and chemokines.

The use of MSCs secretome in cartilage repair also gained its popularity recently [51]. An appealing mechanism by which MSCs enhance repair is the secretion of signaling molecules, which then modify the response of the surrounding endogenous cells [52]. In comparison, dECM mixtures and particles derived from cartilage or other tissues mainly contain matrix proteins, which do not preserve as much bioactivity as stem cell derived products such as secretome. However, the soluble nature of MSCs secretome complicates its administration route. In order to ensure a sustained release of secretome and create chemoattractant gradients to facilitate endogenous cells recruitment, it is essential to customize its administration route or make it insoluble. The engineered MESS not only preserved the natural structure of extracellular matrix, but also inherited the bioactivities of MSCs from their secretome and exosomes during induction, which grants them distinct advantages over other acellular products. The rich and complex set of molecules secreted from stem cells could inherit abilities and functions from their origin cells, grant them stronger bioactivities such as facilitating stem cell chemotaxis and chondrogenesis, and mimic a microenvironment suitable for regeneration through physical interactions and paracrine signals.

To effectively fill and repair the defected cartilage as well as deliver PE-MESS to the defect site, o-alg-THAM/gel hydrogel based on reversible dynamic Schiff base covalent bonds and multiple hydrogen bonding was designed and prepared. The gelation of hydrogel could occur within 15 min after simply blending of o-alg-THAM and gelatin without any other procedures like heating, UV irradiation, etc., which is feasible and suitable for the clinical manipulation. For hydrogels of different formula, the storage modulus (G′) remained stable among the whole frequency range, which indicated that the hydrogel was crosslinked through chemical bonds. Gelation through chemical crosslinking could endow a more stable structure and properties to the hydrogel. Injectable in situ crosslinking self-healing hydrogels could be injected to irregular defects, followed by recovering to an integrated hydrogel at target sites. In situ gelation strategies based on two-component cross-linking through spontaneous bioconjugate chemistry have been developed as injectable hydrogel for cartilage tissue repair [53–56], and it is beneficial to the clinical operation. The designed hydrogel could be easily and smoothly injected through a 23G needle, and firmly attached to the gelatin-covered glass slide or cartilage tissue. Ideal self-healing property was also observed in the designed hydrogel. When implanted into the

defect sites, the hydrogel could recover its original structure even after some damage occurred, indicating the reliability of the hydrogels.

Integration between implanted hydrogels with target tissues is essential for efficient tissue regeneration, particularly for cartilage, because it could effectively facilitate the healing and recovery of damaged tissue [57–59]. Detachment of implanted hydrogel from the defects would possibly cause complications, leading to joint inflammation or other side effects to the surrounding tissues [60,61]. Adhesive property could be achieved based on the formation of chemical bonds between implanted materials and surrounding tissues through various functional groups, such as catechol groups, aldehyde, or physical interactions, like hydrogen bonding, cation-π interactions, etc. For example, biocompatible dopamine hydrochloride, inspired by mussels, has become a widely used raw material in synthetic adhesives [62–64]. However, catechol groups are easy to be oxidized to quinone groups by oxygen, which may limit their long-term adhesion property [65]. For the as-prepared hydrogels, the hydrogel showed a broad adhesion behavior on the surface of plastic tubes, metal and glass, and the adhesive strength is about 1.5–2.0 kPa. Besides, after introducing multiple hydrogen bonding, the hydrogel exhibited enhanced mechanical and adhesion properties. Aldehyde-based adhesives have mild bonding conditions and rapid reactions. Thus, hydrogels with aldehyde groups could effectively binding to the tissues through Schiff-base reaction. Besides, hydrogen-bond-driven hydrogels have excellent adhesion and flexibility, which are beneficial to enhance the mechanical and adhesion properties. The tris(hydroxymethyl)aminomethane (THAM) contains multiple hydrogen bond donors and acceptors, which can form a large number of hydrogen bonds on and inside the hydrogel. Thus, the adhesive hydrogel could also derive from the multiple hydrogen bonds formed between the hydroxyl groups in the hydrogel and the amino groups of the tissue [66,67], and the hydrogen bonds could also be used to strengthen hydrogels due to its relative stability in aqueous condition. Moreover, the strength of multiple hydrogen bonds could be nearly close to that of a covalent bond [68].

Relying on the above multiple adhesion mechanisms, this adhesive hydrogel is expected to exhibit desirable moist adhesion ability and enhanced mechanical properties. In the in vivo experiments, o-alg-THAM/gel hydrogels could be effectively localized into the cartilage defects, and the hydrogel could stably adhere to cartilage defect sites and promote cartilage regeneration.

Stem cell homing is fundamental in the regulation of organogenesis [69,70]. Therefore, in situ strategies for the recruitment of endogenous stem cells provide a promising approach to heal and remodel a tissue such as cartilage. Clinically, treatments such as bone marrow stimulation are already developed based on such concept for cartilage repair, by activating, mobilizing and recruiting stem cells from bone marrow, and yet the clinical outcomes are unsatisfied [71]. Stem cell homing and recruitment requires a cascade of complex signaling events [72,73]. Mimicking these complex events is a crucial step in the design of novel tissue engineering strategies that can enhance the recruitment of endogenous stem and progenitor cells into damaged cartilage. Our findings demonstrated that the composite scaffold with hBMSCs-derived PE-MESS and o-alg/gel hydrogel could enhance endogenous stem cell recruitment and chondrogenic differentiation, and thereby significantly improve the therapeutic outcome of osteochondral defects. The composite scaffold would be suitable as filling material in treatments such as bone marrow stimulation, and offer great potential and benefits for clinical application. The engineered PE-MESS are fabricated through induction of hBMSCs, which present much stronger bioactivities than tissue derived matrices, and have relatively abundant availability. Furthermore, we optimized the production procedure to achieve mass production with standardized quality. We believe that further optimization of this strategy may lead to great clinical translation. The raw materials of the designed hydrogels including gelatin and alginate are natural polymers and easy to obtain, and the modification reaction is feasible and mild. The preparation strategy has the advantages of low cost and convenience for implementing. And the gelation of adhesive hydrogels is easy to handle without any other external triggers, which is beneficial to the clinical operation. Moreover, the scaffold system is designed to be easy to preserve and administrate. Both MESS and hydrogel composition can be long-term stored after lyophilization, which can be easily translated into on-the-shelf products. Upon use, simple rehydration and mixture can make it into a ready-to-use and injectable hydrogel system.

Although the desired therapeutic outcomes of cartilage injury were achieved, there're certain limitations in this study and the as-prepared scaffold needs further optimization. Firstly, different cell types used to prepare MESS were not compared. BMSCs were used in this study as its one of the most well-accepted multipotent seed cells in tissue engineering. However, as MSCs can undergo hypertrophic differentiation after micromass culture, the derived MESS may contain pro-hypertrophy factors, other cell types such as chondrocytes may offer a better solution. Previously, Tang et al. used chondrocyte secretome enriched microparticles to facilitate the chondrogenesis of BMSCs and reduce hypertrophy [74]. Further investigation is needed to explore alternative cell sources for engineering MESS. Secondly, although the designed hydrogels exhibited enhanced mechanical and adhesive properties compared to original o-alg/gel hydrogel, the wet adhesion strength is still not remarkable. As previously mentioned, catechol-based hydrogels showed strong adhesion to different kinds of surfaces and even wet substrates [75]. However, catechol moieties inevitably and easily undergo oxidation to quinone, resulting in a loss of adhesiveness. In view of this situation, Xu [76] et al. developed a bio-inspired hydrogel based on thiourea-catechol coupling between the NCSN (thiourea) and catechol groups grafted to HA backbone. The presence of the reducing NCSN groups helped reduce the excessive oxidization of catechol groups, thus preserving the adhesiveness of the hydrogels. Besides, removing interfacial water on wet tissues is also an effective approach to achieving wet adhesion. Peng [77] et al. designed a kind of polyethyleneimine/polyacrylic acid (PEI/PAA) powder that can in situ form physically cross-linked hydrogels on wet tissues within 2 s. Superficially deposited PEI/PAA powder can absorb interfacial water to form tight contact with various wet substrates. From this point of view, the introduction of new materials components and adhesion mechanism is an ideal strategy to enhance the wet adhesive properties of our hydrogels.

4. Conclusion

This study developed a cell free strategy for articular cartilage repair by combining an injectable, adhesive and self-healable o-alg-THAM/gel hydrogel system as scaffolds and a biophysio-enhanced hBMSCs-derived MESS as bioactive supplement. The engineered MESS and PE-MESS facilitates stem cell recruitment, migration, aggregation, and chondrogenesis, and modulates cell inflammation response The o-alg-THAM/gel hydrogel system presented desirable biocompatibility and physical properties, which harvested the biological functions of the MESS and yet avoided its weaknesses such as weak mechanical properties. This combination presented superior bioactivities in vitro and in vivo, which could potentially achieve comprehensive and balanced therapeutic effects during cartilage defect healing in the knee, providing a promising strategy for cartilage tissue engineering.

5. Experimental section/methods

All experiments were approved by the Animal Research Ethics Committee of the Chinese University of Hong Kong (AEEC number:20-225-HMF).

5.1. Hydrogel preparation

5.1.1. Materials

Sodium alginate (Viscosity 501 cP at 1%) and sodium periodate

($NaIO_4$) were purchased from Shanghai Aladdin Biochemical Technology Co., LTD. Ethyl alcohol (99.9%) and ethylene glycol (99.8%) were obtained from Supelco, Merck. All of the chemicals are used directly without further treatments. Dialysis bag (MWCO = 3500 Da) was obtained from Vake.

5.1.2. Preparation of oxidized alginate

Oxidized alginate was prepared according to previous studies [78]. Briefly, 4 g of sodium alginate powder was dispersed in 25 mL of ethanol under continuous stirring. Subsequently, a solution containing different amounts of $NaIO_4$ (2 g, 3 g and 4 g, respectively, as listed in Table S1) in 25 mL of ultrapure water was added dropwise into the previous solution. The suspension was stirred for different time under dark environment. After that, the reaction was stopped by adding 5 mL of ethylene glycol and allowed to react for further half an hour. The suspension was then dialyzed for 3 days against ultrapure water and the water was changed twice a day. Then the obtained solution was lyophilized.

Hydroxylamine hydrochloride method was conducted to determine the amounts of aldehyde groups of different groups of o-alg. In brief, 10 mL of 0.5% o-alg was prepared and the pH was adjusted to 4. Then hydroxylamine hydrochloride solution (0.3 mol/L, pH 4) was added dropwise to the o-alg solution under continuous stirring. The pH value of the mixture solution was monitored by a precision pH meter. 0.1 mol/L of NaOH solution was added dropwise and carefully to maintain the pH of the mixture solution at a constant value of 4. The measurement stopped when the pH of the mixture solution was not change after continuous addition of hydroxylamine hydrochloride solution. The total amounts of NaOH solution consumed during the measurement were recorded. Different reaction conditions of o-alg were listed in Table S1.

5.1.3. Preparation of THAM-grafted oxidized alginate (o-alg-THAM)

In order to keep the amounts of residual aldehyde groups same after reacted with THAM, here o-alg with 0.00325, 0.0042, 0.00515 and 0.00635 mol/g aldehyde groups were furtherly used. A certain amount of o-alg was dissolved into dH2O. Then relevant amount of THAM (listed in Table 1) was added into the o-alg solution and pH of the mixture solution was adjusted to 7.2. The reaction was continued for 2 h and then the suspension was dialyzed for 3 days against ultrapure water. The water was changed twice a day. Then the obtained solution was lyophilized to obtain o-alg-THAM.

5.1.4. Preparation of o-alg/gel and o-alg-THAM/gel hydrogels

Gelatin was dissolved into distilled H_2O at 37 °C with concentration of 8 wt%. The o-alg and o-alg-THAM with different THAM graft amounts were dissolved into dH_2O to obtain homogenous solution with concentration of 8%. For the preparation of o-alg/gel hydrogel, o-alg solution and gelatin solution were thoroughly mixed in the volume ratio of 1:1 to prepare precursor mixture solution. The pH value of the precursor solution was adjusted to 7.2 using $NaHCO_3$ solution. Then the solution was transferred into a mould, such as cell culture plate. After a few minutes, o-alg/gel hydrogels could be prepared. For the preparation of o-alg-THAM/gel hydrogel, the procedure was almost the same as above, except that the o-alg-THAM was added instead of o-alg.

In order to visually illustrate the injectability and moist adhesion of the o-alg-THAM/gel hydrogels, the hydrogels were firstly injected onto a gelatin-coated glass slide through a 23G needle under normal conditions. Then the hydrogels were injected onto a gelatin-coated glass slide under moisture condition. The entire procedure was recorded.

5.2. Characterizations of o-alg/gel and o-alg-THAM/gel hydrogels

5.2.1. Gelation time

The gelation time of each group of hydrogels was measured by the published inverted vial method. The time that the hydrogel precursor solution taken to stop flowing under 37 °C when they were inverted by 180° was recorded to compare the gelation efficiency of different groups of hydrogels.

5.2.2. Crosslinking degree of hydrogels

Degree of crosslinking of hydrogels was evaluated by ninhydrin assay [79]. This assay determined the amount of free amino groups of gelatin presented in the hydrogel after crosslinking with o-alg or o-alg-THAM. Briefly, 0.5 mL of hydrogel precursor solution was added into a 1.5 mL centrifuge tube and the hydrogel was then obtained. After that, the hydrogel was smashed and then 1 mL of ninhydrin solution (0.5 wt%) was added. The mixture was heated to 70 °C for 30 min. After that, the solution was cooled down to room temperature and centrifuged for 5 min with relative centrifugal field of 5000 g. After that, the optical absorbance of the supernatant was recorded with a spectrophotometer at 570 nm. The amount of free amino groups in the same amount of gelatin before hydrogel gelation was also measured. Glycine solutions with various known concentrations (0.004–0.02 mol/L) were used as standard of concentrations of free amino groups. The crosslinking degree was determined as:

$$\text{crosslinking degree } (\%) = [n(gel) - n(h)] / n(gel) \times 100\%.$$

Where n(gel) is the molar amount of free amino groups in gelatin before hydrogel gelation and n(h) is the molar amount of free amino group in the crosslinked hydrogel.

5.2.3. Rheology measurements

The storage modulus (G') and loss modulus (G") of different groups of the as-prepared hydrogels were measured using a rheometer (MCR 302, Anton Paar, Austria), which was equipped with an 8 mm parallel plate.

5.2.3.1. Frequency sweep. Frequency sweep of 0.01–10 Hz with a fix strain of 1% at 37 °C was carried out. Briefly, different groups of hydrogels were prepared with dimensions of Φ8mm x 3 mm and placed onto the down plate of the rheometer. Then the top plate was lowered to make a slight contact with the surface of the tested hydrogel. Then frequency sweep was carried out.

5.2.3.2. Time sweep with cyclic strain and splicing tests. The rheology test was used to investigate the self-healing property of the hydrogels. A time sweep measurement was conducted to study the recovery properties of the hydrogel samples in response to applied cyclic strain. Different groups of hydrogels were prepared with dimensions of Φ8mm x 3 mm and placed onto the down plate of the rheometer. Then the top plate was lowered to make a slight contact with the surface of the hydrogel. The strain was changed from 1% to 100% (60 s per stage) under a constant frequency of 1 Hz.

The self-healing properties of the hydrogels were also monitored by schematic photographs. Two blocks of disk-shaped hydrogel were prepared as mentioned above. One of them was stained with methylene blue. Then the two blocks of hydrogel were both cut into halves. The two half pieces of the original and stained hydrogel were brought into contact at 37 °C under moist conditions for 1 h without any additional external stimulus. The optical images of self-healed hydrogel were recorded.

5.2.3.3. Adhesive properties. The adhesive properties of the as-prepared hydrogels were determined through the lap-shear adhesion measurements. By placing the hydrogel between tested objects with the overlapped contact area dimensions of 25 mm × 20 mm x 1 mm, the samples were pressed slightly for 10 s to enhance the adhesion. Then the test samples were kept in a 37 °C incubator for 15 min. Subsequently, the samples were pulled to failure and the max load was recorded.

5.3. Engineering microspheres of ECM and solidified secretome (MESS) from hBMSCs aggregates

5.3.1. Induction of hBMSCs chondrogenic microspheres

Human bone marrow derived mesenchymal stem cells (hBMSCs) from 3 donors (purchased from Millipore, Temecula, USA) were used. hBMSCs were expanded to passage 4 using αMEM supplemented with 10% FBS and 1% penicillin/streptomycin.

After cell expansion, hBMSCs in suspension were seeded into 6-well plates (4×10^6 cells in 5 mL suspension per well) equipped with 3D CoSeedis™ Chip200 microwell system (ABC-C200, abc Biopply). The plates were then subjected to centrifugation at 300*g* for 5 min to obtain hBMSCs aggregates. The obtained cell aggregates contained approximately 20,000 cells/aggregate. hBMSCs aggregates were then subjected to chondrogenic differentiation induction for 14 days. Chondrogenic induction medium containing Dulbecco's modified Eagle's medium (DMEM) supplemented with 10 ng/mL transforming growth factor-β1 (PerproTech), 10^{-7}M dexamethasone, 50 mg/mL ascorbate-2-phosphate, 40 mg/mL proline, 100 mg/mL pyruvate (all from Sigma-Aldrich), and 1:100 diluted (ITS + Premix) (Becton Dickinson) was replaced every day, and cell aggregates after 14 days of induction were collected for decellularization.

5.3.2. Enhancing the quality of hBMSCs chondrogenic microspheres with pulsed electromagnetic fields (PEMF)

During chondrogenic induction of hBMSCs aggregates, a pulsed electromagnetic field stimulation was utilized to enhance the quality of secreted matrix and secretome by hBMSCs according to our previous publication [27]. Our previous study has demonstrated that PEMF stimulation with an FDA approved signal (Physio Signal, 10T/s, 15 Hz, Orthofix Medical Inc, USA) could promote BMSCs chondrogenic differentiation and mitigate cell hypertrophy process. Therefore, we hypothesized that with the daily treatment of PEMF could effectively enhance the quality of MESS. From day 1 of chondrogenic induction of hBMSCs aggregates, daily PEMF treatment (3 h/day) was given to the cells using an in vitro PEMF device (Orthofix Medical Inc.) for 14 days. Obtained cell aggregates were collected for decellularization.

5.3.3. Decellularization of hBMSCs chondrogenic microspheres

At the completion of culture period, cell aggregates were collected and subjected to a decellularization treatment. The decellularization procedure was modified from previously published protocols with the purpose of maximum preservation of bioactivities [80,81]. Briefly, cell aggregates were firstly subjected to 5 five cycles of 2 min freezing in liquid nitrogen and 10 min thawing in PBS at 37 °C for cell devitalization. The chemical procedure consisted on incubation in a detergent solution containing 0.25% Triton X-100 and 10 mM NH_4OH at 37 °C for 1 h followed by treatment with 50 units/mL deoxyribonuclease (DNase) I and 50 mg/mL ribonuclease (RNase) A (Invitrogen) for 2 h. After several washes with PBS, the engineered MESS and PE-MESS were obtained, collected in double deionized water (ddH_2O), lyophilized, and stored at −20 °C for future usage.

5.3.4. Decellularization of cartilage matrix microparticles

Bovine cartilage was shattered and decellularized. Cartilage was washed and shattered into small particles with a tissue homogenizer in phosphate-buffered saline (PBS) containing 3.5% (w/v) phenylmethyl sulfonylfluoride (Merck, Darmstadt, Germany) and 0.1% (w/v) EDTA (Sigma, Poole, UK) to inhibit protease activity. Cartilage particles prepared were then incubated in 1% TritonX-100 in hypotonic Tris–HCl with gentle agitation for 12 h at 4 °C, they were rinsed several times with deionizer water, then incubated for 12 h in DNase (Sigma-Aldrich, NJ, United States) and RNase (Sigma-Aldrich, NJ, United States) with agitation at 37 °C. After several washes with PBS, the decellularized cartilage matrix (tECM) microparticles were obtained, collected in double deionized water (ddH_2O), lyophilized, and stored at −20 °C for future usage.

5.3.5. DNA quantification

To determine the DNA content after decellularization, MESS were lysed using digestion buffer (10×10^{-3} m Tris-HCl and 1×10^{-3} m EDTA) with 0.1 mg/mL proteinase K (Sigma-Aldrich) at 50 °C overnight. The amount of DNA in the lysates was quantified using a Quant-iT PicoGreen dsDNA quantitation kit (Thermo Fisher Scientific) according to the manufacturer's instructions. Briefly, Quant-iT PicoGreen reagent was added to the lysates and incubated for 5 min, and fluorescence was measured using a microplate reader (SpectraMax iD3, Molecular Devices, Sunnyvale, CA, USA) at an excitation wavelength of 480 nm and an emission wavelength of 520 nm. The absolute DNA content was determined according to a standard curve generated using lambda DNA (Thermo Fisher Scientific).

5.3.6. Determination of glycosaminoglycan content

The glycosaminoglycan (GAG) content of the treated discs was assessed by the standard DMMB assay. Briefly, MESS before or after decellularization were lyophilized to a constant weight and then digested with Protease K solution in phosphate buffer (0.05 mg/mL) (Roche, Germany) at 60 °C for 24 h. The absorbance values of the samples were read at 535 and 595 nm immediately upon the addition of the 1,9-dimethylene blue solution. The amount of GAGs was calculated with reference to a standard curve made by serial dilutions of chondroitin-4-sulfate (C4S) (Sigma–Aldrich, USA). The GAG content was expressed as the amount of C4S per mg dry mass.

5.4. Proteomics on MESS and PE-MESS and bioinformatic analysis

MESS and PE-MESS engineered with hBMSCs from 3 different donars were subjected to protomics analysis using iTRAQ. Proteins were identified and quantified using the previously described ITRAQ method [82]. Briefly, samples were precipitated by acetone at −20 °C overnight to obtain a reduced and alkylated protein mixture. A 100 μg of each sample solution is digested with Trypsin Gold (Promega, Madison, WI, USA). After digestion, peptides were labeled with an 8-plex iTRAQ reagent (Applied Biosystems, USA) according to the manufacturer's protocol. An LC-20AB HPLC pump system (Shimadzu, Kyoto, Japan) was used to separate each sample into 20 fractions. Each fraction was resuspended, then the peptides are subjected to nanoelectrospray ionization followed by tandem mass spectrometry (MS/MS) in a QEXACTIVE (Thermo Fisher Scientific, San Jose, CA, USA) coupled online to the HPLC. Protein identifications were performed by using Maxquant with a search engine. Proteins with 2 fold change and Q value less than 0.05 were determined as differentially expressed protein in single replicate.

For down-stream analysis, output was exported to Excel and proteins were annotated using Uniprot (https://www.uniprot.org/) and their subcellular locations were identified. Secreted proteins were separately shortlisted. The function of listed proteins was then annotated by Gene Ontology (GO), Pathway analysis was performed using the Kyoto Encyclopedia of Genes and Genomes (KEGG) database in DAVID Bioinformatics software (Resources 6.8, https://david.ncifcrf.gov) with FDR <0.05. The heat map was generated by program R (v3.6.1, www.r-project.org). Protein-protein interaction analysis (PPI) and pathway interactions were analyzed using the ClueGO plug-in of Cytoscape and STRING (v. 11.0; https://string-db.org).

5.5. In vitro evaluation of MESS and PE-MESS hydrogels

5.5.1. 1Protein release assay

Blank hydrogels, hydrogels supplemented with bovine serum albumin (BSA, 10 μg/mL, Sigma-Aldrich, A7030), MESS hydrogels and PE-MESS hydrogels were each formed in 96 well-plates. After polymerization for 40 min, hydrogels were overlaid with 50 μl PBS. 30 μL of the supernatant was collected at various time-points and replenished with

fresh PBS. Proteins released into the supernatant from hydrogels were quantified with the Pierce™ Rapid Gold BCA Kit (Life Technologies, USA). Values from blank hydrogels served for normalization, and the total amount of released protein was calculated.

5.5.2. MSCs migration analysis

The effects of MESS and PE-MESS on rBMSCs migration were evaluated using a 24-well transwell. Blank hydrogels, MESS hydrogels and PE-MESS hydrogels (n = 3) were each formed on the top of the transwell membrane. Then, the transwell setups were placed in a 24-well plate. The volume of each hydrogel was 50 μL. Next, 100 μL of medium containing rat GFP-BMSCs (2×10^6/mL) were added to the top of the hydrogels, and 700 μL of growth media were added to the 24-well plates. After 12 h of incubation at 37 °C, the hydrogels were fixed with 4% paraformaldehyde. The MESS and PE-MESS were labeled with red fluorescence with an immunofluorescence protocol. Briefly, the hydrogels were incubated with primary antibody anti-aggrecan (sc-33695, 1:500) for 16 h at 4 °C, and washed 5 times with PBS for 5 min each wash. The hydrogels were then incubated with secondary antibody Alexa Fluor 647 (Invitrogen A-21242, 1:500) overnight at 4 °C, and washed 5 times with PBS for 10 min each wash. The nuclei were stained with DAPI (Thermo Fisher Scientific, 62,248, 1 μg/ml). Confocal micrographs were obtained to visualize the distribution of the cells in the hydrogels. Quantitative analysis was performed on the obtained confocal images with ImageJ. Number of MSCs infiltrated into the hydrogels and the maximum cell infiltration depth were calculated.

5.5.3. Effects of MESS and PE-MESS hydrogels on chondrogenic differentiation of BMSCs

The effect of MESS and PE-MESS on rat and human BMSCs was studied in a transwell system (Fig. 4. F). rBMSCs and hBMSCs from 3 different donors obtained from primary culture were expanded to passage 4 using αMEM supplemented with 10% FBS and 1% penicillin/streptomycin.

Micromasses of rBMSCs and hBMSCs from 3 different donors constructed by 2×10^5 cells were obtained as previous established [83]. Blank hydrogels, MESS hydrogels and PE-MESS hydrogels, 30 μL each, were formed on the top of the transwell membrane. Then, the transwell setups were placed in a 24-well plate. rBMSCs and hBMSCs micromasses and 770 μL of chondrogenic induction medium were added to the 24-well plates. The chondrogenesis induction medium was replaced every 3 days. The cell micromasses were harvested at days 14 upon chondro-induction for qPCR analysis and staining.

5.5.4. Effects of MESS and PE-MESS hydrogels on the regulation of macrophages

The regulatory effects of MESS and PE-MESS on macrophages was studied in a transwell system (Fig. 4. J). Blank hydrogels, MESS hydrogels and PE-MESS hydrogels in transwells were prepared as stated above. Rat NR8383 macrophages (CRL-2192, ATCC) were cultured in growth medium containing Ham's F–12 K Medium and 15% heat-inactivated FBS and used for induction of inflammatory and anti-inflammatory macrophages. For inflammatory phenotype induction, NR8383 macrophages were cultured in fusion medium containing 10 ng/ml lipopolysaccharide (LPS) and 500 U/ml IFN-γ (PeproTech) in growth medium for 24 h. For anti-inflammatory phenotype induction, NR8383 macrophages were cultured in fusion medium containing 10 ng/ml IL-4 (404-ML-010/CF; R&D Systems, Minnesota, USA) in growth medium for 24 h. The obtained inflammatory and anti-inflammatory macrophages were seeded to the 24-well plates (2×10^4 cells per well) and 770 μL of growth medium were added. The supernatant of medium was collected after 4 days of cell culture and subjected to enzyme-linked immunosorbent assay (ELISA) to detect the secretion of interleukin 1β (IL-1β), tumor necrosis factor α (TNF-α), interleukin 10 (IL-10) and transforming growth factor β1 (TGF-β1) with commercial ELISA kit (R&D Systems) [84].

5.6. Subcutaneous implantation

Blank hydrogel and hydrogels functionalized with MESS, PE-MESS were prepared as previous described. SD rats (male, 8 weeks old) were anesthetized, and blank hydrogels, MESS hydrogels and PE-MESS hydrogels, 100 μL each, were transplanted subcutaneously into the back of the rats by injection with a 23G needle according to the grouping (Fig. 5. A). Samples were collected at day 7 postoperative and subjected to fixation with 4% PFA. Histological and immunofluorescence staining were performed to evaluate the biocompatibility and bioactivities of hydrogels in vivo.

5.7. Osteochondral defect

Three-month-old SD rats (male, weight 300–350 g, n = 100) were divided into 5 groups and subjected to rat osteochondral defect surgery as previously described [85]. In brief, the osteochondral defects were created using a 1.5 mm diameter dental drill in the center of the left femoral trochlear groove with 1.5 mm in depth. The defect was rinsed with 0.9% saline and the debris was removed using a curette and implanted with different biomaterials according to different groups. The osteochondral defects were transplanted with four types of hydrogels: blank hydrogels, hydrogels functionalized with decellularized cartilage matrix microparticles (tECM hydrogels), MESS hydrogels, and PE-MESS hydrogels, respectively. Rats in negative control group received no hydrogel implantation. Decellularized cartilage matrix microparticles loading hydrogels were used as positive control as its a well-established and widely reported strategy [43–46]. Rats were terminated after 4 and 8 weeks with pentobarbital overdose. The left femur of the rats was collected and were fixed in 10% buffered formalin. Samples were decalcified in a 10% solution of buffered ethylenediaminetetraacetic acid (EDTA, Sigma-Aldrich, USA). Histological and immunohistochemical staining were performed to determine the healing outcome of osteochondral defect.

5.8. Quantitative real-time PCR

Total cellular RNA was extracted from hydrogel samples with MiniBEST universal RNA extraction kit (Takara, Japan), and reversely transcribed into cDNA with M-MLV reverse transcriptase according to the manufacturer's instructions (Takara, Japan). Real-time PCR was performed using the Step One Plus Real-Time PCR System (Applied Biosystems, USA). 10 μl reaction volume was consisted of 1 μl cDNA template diluted with Milli-Q water, 5 μl SYBR-Green Master Mix (2X, Applied Biosystems, USA), 3.4 μl PCR grade water, and 0.6 μl of primer (10 μM). The amplification procedure was carried out as follows: first at 95 °C for 5 min, and then 40 cycles of 95 °C for 15 s and 60 °C for 60 s. Primer sequences were shown in Table 2. The relative quantification of gene expression was analyzed with the values of $2^{-\Delta\Delta CT}$, normalized to the GAPDH expression.

5.9. Safranin O & fast green staining

After deparaffinized and hydrated, sections of samples were stained with 0.05% fast green (Sigma-Aldrich) solution for 5 min. Sections were rinsed with 1% acetic acid solution for 15 s and stained with 0.1% safranin O (Sigma- Aldrich) solution for 5 min. Residual dye was removed using 95% ethanol and absolute ethanol for 2 min each.

5.10. Histology, immunofluorescence and immunohistochemistry staining

H&E, immunofluorescence (IF) and immunohistochemistry (IHC) staining was performed using a standard protocol as previously reported [86]. Primary antibodies are as follows: mouse anti-rat Collagen type II (Col II; ab34712, 1:100, Abcam, UK), rabbit anti-rat Collagen type X (Col X; ab49945, 1:200, Abcam, UK), rabbit anti-rat CD68 (ab283654; 1:200,

Table 2
Primers for quantitative real-time reaction (qPCR).

Gene Name	Forward (5′–3′)	Reverse (5′–3′)
Rat Primers		
GAPDH	AGCCCAGAACATCATCCCTG	CACCACCTTCTTGATGTCATC
Sox-9	AGAGCGTTGCTCGGAACTGT	TCCTGGACCGAAACTGGTAAA
Col 2a1	AACCCAAAGGACCCAAATAC	CCGGACTGTGAGGTTAGGAT
ACAN	TTGTGACTCTGCGGGTCATC	GTCCCTAGGAGGGCCTTCAG
MMP13	AGGCCTTCAGAAAAGCCTTC	GAGCTGCTTGTCCAGGTTTC
Col 10a1	ATATCCTGGGGATCCAGGTC	TCCAGGTTCACCTCTTGGAC
Runx2	GAACCAAGAAGGCACAGAC	AATGCGCCCTAAATCACTG
Human Primers		
GAPDH	CCAGGGCTGCTTTTAACTCTGGTAAAGTGG	ATTTCCATTGATGACAAGCTTCCCGTTCTC
Sox-9	TGGGCAAGCTCTGGAGACTTC	ATCCGGGTGGTCCTTCTTGTG
Col 2a1	CGGCTTCCACACATCCTTAT	CTGTCCTTCGGTGTCAGGG
ACAN	TCTTGGAGAAGGGAGTCCAACTCT	ACAGCTGCAGTGATGACCCTCAGA
MMP13	AAGGAGCATGGCGACTTCT	TGGCCCAGGAGGAAAAGC
Col 10a1	GTGGACCAGGAGTACCTTGC	CATAAAAGGCCCACTACCCA
Runx2	GACAAGCACAAGTAAATCATTGAACTACAG	GTAAGGCTGGTTGGTTAAGAATCTCTG

Abcam, UK), rabbit anti-rat CD11b (ab133357; 1:200, Abcam, UK), rabbit anti-rat CD44 (ab41478; 1:200, Abcam, UK), mouse anti-rat CD90 (ab181469; 1:200, Abcam, UK). A horseradish peroxidase-streptavidin detection system (Dako, USA) was used for IHC staining. ImageJ was used to perform the semi-quantitative and quantitative analysis of obtained pictures.

5.11. Cartilage repair analysis by the wakitani scoring system

Rat cartilage sections of each defect at week 4 and 8 after hydrogel implantation were scored using Safranin O & Fast Green staining to define the region of cartilage in newly formed surface tissue ($n = 10$ per group). Histology sections were blindly scored by three independent researchers based on a previously established scoring system by Wakitani et al. [47].

5.12. Statistical analysis

Data was presented as mean ± standard deviation. All the quantitative and semi-quantitative data were analyzed using SPSS 18.0 software for windows (SPSS, Chicago, IL, USA). Parameters were analyzed by analysis of variance (ANOVA). One-way ANOVA and Tukey multiple comparison was used for comparison among groups and two-way ANOVA and Tukey multiple comparison was used for comparison among groups and time factor. $P < 0.05$ was considered as statistically significant.

CRediT authorship contribution statement

Yucong Li: Conceptualization, Data curation, Formal analysis, Investigation, Methodology, Project administration, Writing – review & editing. **Linlong Li:** Data curation, Formal analysis, Investigation, Methodology, Writing – original draft. **Ming Wang:** Data curation, Formal analysis, Investigation. **Boguang Yang:** Investigation, Resources, Software. **Baozhen Huang:** Investigation, Resources, Software. **Shanshan Bai:** Investigation, Methodology. **Xiaoting Zhang:** Investigation, Methodology. **Nan Hou:** Methodology, Resources. **Haixing Wang:** Investigation, Methodology. **Zhengmeng Yang:** Methodology. **Chong Tang:** Resources. **Ye Li:** Resources. **Wayne Yuk-Wai Lee:** Conceptualization, Supervision. **Lu Feng:** Supervision, Validation, Writing – review & editing. **Micky D. Tortorella:** Supervision, Validation, Writing – review & editing. **Gang Li:** Conceptualization, Funding acquisition, Project administration, Resources, Writing – review & editing.

Declaration of competing interest

The authors have no conflicts of interest to disclose in relation to this article.

Acknowledgements

This work was supported by grants from the National Natural Science Foundation of China (82172430 and 82272505), University Grants Committee, Research Grants Council of the Hong Kong Special Administrative Region, China (14108720, 14121721, 14202920, N_CUHK472/22, C7030-18G, T13-402/17-N and AoE/M-402/20), Heath Medical Research Fund (HMRF) Hong Kong (16170951, 17180831, 08190416 and 09203436), Hong Kong Innovation Technology Commission Funds (PRP/050/19FX). This study also received support from the research funds from Health@InnoHK program launched by Innovation Technology Commission of the Hong Kong SAR, PR China. The authors would like to acknowledge Orthofix Medical Inc. USA for providing the PEMF devices for this study.

Appendix A. Supplementary data

Supplementary data to this article can be found online at https://doi.org/10.1016/j.bioactmat.2023.05.003.

References

[1] T.A. Holland, J.K. Tessmar, Y. Tabata, A.G. Mikos, Transforming growth factor-β1 release from oligo (poly (ethylene glycol) fumarate) hydrogels in conditions that model the cartilage wound healing environment, J. Contr. Release 94 (1) (2004) 101–114.
[2] A. Gomoll, J. Farr, S. Gillogly, J. Kercher, T. Minas, Surgical management of articular cartilage defects of the knee, JBJS 92 (14) (2010) 2470–2490.
[3] J.R. Steadman, K.K. Briggs, J.J. Rodrigo, M.S. Kocher, T.J. Gill, W.G. Rodkey, Outcomes of microfracture for traumatic chondral defects of the knee: average 11-year follow-up, Arthrosc. J. Arthrosc. Relat. Surg. 19 (5) (2003) 477–484.
[4] B. Chuckpaiwong, E.M. Berkson, G.H. Theodore, Microfracture for osteochondral lesions of the ankle: outcome analysis and outcome predictors of 105 cases, Arthrosc. J. Arthrosc. Relat. Surg. 24 (1) (2008) 106–112.
[5] J. Lu, X. Shen, X. Sun, H. Yin, S. Yang, C. Lu, Y. Wang, Y. Liu, Y. Huang, Z. Yang, X. Dong, C. Wang, Q. Guo, L. Zhao, X. Sun, S. Lu, A.G. Mikos, J. Peng, X. Wang, Increased recruitment of endogenous stem cells and chondrogenic differentiation by a composite scaffold containing bone marrow homing peptide for cartilage regeneration, Theranostics 8 (18) (2018) 5039–5058.
[6] A. Gobbi, G. Karnatzikos, A. Kumar, Long-term results after microfracture treatment for full-thickness knee chondral lesions in athletes, Knee Surg. Sports Traumatol. Arthrosc. 22 (2014) 1986–1996.
[7] K. Bankoti, A.P. Rameshbabu, S. Datta, P. Goswami, M. Roy, D. Das, S.K. Ghosh, A. K. Das, A. Mitra, S. Pal, Dual functionalized injectable hybrid extracellular matrix hydrogel for burn wounds, Biomacromolecules 22 (2) (2020) 514–533.
[8] Y.S. Kim, M. Majid, A.J. Melchiorri, A.G. Mikos, Applications of decellularized extracellular matrix in bone and cartilage tissue engineering, Bioeng. Trans. Med. 4 (1) (2019) 83–95.

[9] S.F. Badylak, D. Taylor, K. Uygun, Whole-organ tissue engineering: decellularization and recellularization of three-dimensional matrix scaffolds, Annu. Rev. Biomed. Eng. 13 (2011) 27–53.
[10] S.F. Badylak, D.O. Freytes, T.W. Gilbert, Extracellular matrix as a biological scaffold material: structure and function, Acta Biomater. 5 (1) (2009) 1–13.
[11] A.I. Hoch, V. Mittal, D. Mitra, N. Vollmer, C.A. Zikry, J.K. Leach, Cell-secreted matrices perpetuate the bone-forming phenotype of differentiated mesenchymal stem cells, Biomaterials 74 (2016) 178–187.
[12] E.P. Brennan, X.H. Tang, A.M. Stewart-Akers, L.J. Gudas, S.F. Badylak, Chemoattractant activity of degradation products of fetal and adult skin extracellular matrix for keratinocyte progenitor cells, J. Tissue Eng. Regen. Med. 2 (8) (2008) 491–498.
[13] J.E. Reing, L. Zhang, J. Myers-Irvin, K.E. Cordero, D.O. Freytes, E. Heber-Katz, K. Bedelbaeva, D. McIntosh, A. Dewilde, S.J. Braunhut, Degradation products of extracellular matrix affect cell migration and proliferation, Tissue Eng. 15 (3) (2009) 605–614.
[14] Q. Meng, Z. Man, L. Dai, H. Huang, X. Zhang, X. Hu, Z. Shao, J. Zhu, J. Zhang, X. Fu, A composite scaffold of MSC affinity peptide-modified demineralized bone matrix particles and chitosan hydrogel for cartilage regeneration, Sci. Rep. 5 (1) (2015) 1–14.
[15] X. Zheng, F. Yang, S. Wang, S. Lu, W. Zhang, S. Liu, J. Huang, A. Wang, B. Yin, N. Ma, Fabrication and cell affinity of biomimetic structured PLGA/articular cartilage ECM composite scaffold, J. Mater. Sci. Mater. Med. 22 (2011) 693–704.
[16] R.O. Hynes, The extracellular matrix: not just pretty fibrils, Science 326 (5957) (2009) 1216–1219.
[17] C. Hughes, L. Radan, W.Y. Chang, W.L. Stanford, D.H. Betts, L.-M. Postovit, G. A. Lajoie, Mass spectrometry–based proteomic analysis of the matrix microenvironment in pluripotent stem cell culture, Mol. Cell. Proteomics 11 (12) (2012) 1924–1936.
[18] M. Ding, H. Tegel, Å. Sivertsson, S. Hober, A. Snijder, M. Ormö, P.-E. Strömstedt, R. Davies, L. Holmberg Schiavone, Secretome-based screening in target discovery, SLAS Discovery 25 (6) (2020) 535–551.
[19] M. Kawecki, W. Łabuś, A. Klama-Baryla, D. Kitala, M. Kraut, J. Glik, M. Misiuga, M. Nowak, T. Bielecki, A. Kasperczyk, A review of decellurization methods caused by an urgent need for quality control of cell-free extracellular matrix'scaffolds and their role in regenerative medicine, J. Biomed. Mater. Res. B Appl. Biomater. 106 (2) (2018) 909–923.
[20] C.H. Chang, S.T. Loo, H.L. Liu, H.W. Fang, H.Y. Lin, Can low frequency electromagnetic field help cartilage tissue engineering? J. Biomed. Mater. Res. Part A: An Official Journal of The Society for Biomaterials, The Japanese Society for Biomaterials, and The Australian Society for Biomaterials and the Korean Society for Biomaterials 92 (3) (2010) 843–851.
[21] M.D. Mattei, A. Caruso, F. Pezzetti, A. Pellati, G. Stabellini, V. Sollazzo, G. C. Traina, Effects of pulsed electromagnetic fields on human articular chondrocyte proliferation, Connect. Tissue Res. 42 (4) (2001) 269–279.
[22] S. Anbarasan, U. Baraneedharan, S.F. Paul, H. Kaur, S. Rangaswami, E. Bhaskar, Low dose short duration pulsed electromagnetic field effects on cultured human chondrocytes: an experimental study, Indian J. Orthop. 50 (1) (2016) 87.
[23] F. Vincenzi, M. Targa, C. Corciulo, S. Gessi, S. Merighi, S. Setti, R. Cadossi, M. B. Goldring, P.A. Borea, K. Varani, Pulsed electromagnetic fields increased the anti-inflammatory effect of A2A and A3 adenosine receptors in human T/C-28a2 chondrocytes and hFOB 1.19 osteoblasts, PLoS One 8 (5) (2013).
[24] J. Li, Y. Liu, Y. Zhang, B. Yao, Z. Li, W. Song, Y. Wang, X. Duan, X. Yuan, X. Fu, Biophysical and biochemical cues of biomaterials guide mesenchymal stem cell behaviors, Front. Cell Dev. Biol. 9 (2021), 640388.
[25] K. Spanoudes, D. Gaspar, A. Pandit, D.I. Zeugolis, The biophysical, biochemical, and biological toolbox for tenogenic phenotype maintenance in vitro, Trends Biotechnol. 32 (9) (2014) 474–482.
[26] S. Ding, P. Kingshott, H. Thissen, M. Pera, P.Y. Wang, Modulation of human mesenchymal and pluripotent stem cell behavior using biophysical and biochemical cues: a review, Biotechnol. Bioeng. 114 (2) (2017) 260–280.
[27] Y. Li, L. Li, Y. Li, L. Feng, B. Wang, M. Wang, H. Wang, M. Zhu, Y. Yang, E. I. Waldorff, Enhancing cartilage repair with optimized supramolecular hydrogel-based scaffold and pulsed electromagnetic field, Bioact. Mater. 22 (2023) 312–324.
[28] D. Albani, A. Gloria, C. Giordano, S. Rodilossi, T. Russo, U. D'Amora, M. Tunesi, A. Cigada, L. Ambrosio, G. Forloni, Hydrogel-Based Nanocomposites and Mesenchymal Stem Cells: A Promising Synergistic Strategy for Neurodegenerative Disorders Therapy, Sci World J, 2013.
[29] J.Q. Wang, F.J. Zhang, W.P. Tsang, C. Wan, C. Wu, Fabrication of injectable high strength hydrogel based on 4-arm star PEG for cartilage tissue engineering, Biomaterials 120 (2017) 11–21.
[30] E.A. Appel, J. del Barrio, X.J. Loh, O.A. Scherman, Supramolecular polymeric hydrogels, Chem. Soc. Rev. 41 (18) (2012) 6195–6214.
[31] H. Jung, J.S. Park, J. Yeom, N. Selvapalam, K.M. Park, K. Oh, J.-A. Yang, K.H. Park, S.K. Hahn, K. Kim, 3D tissue engineered supramolecular hydrogels for controlled chondrogenesis of human mesenchymal stem cells, Biomacromolecules 15 (3) (2014) 707–714.
[32] Q. Feng, K. Wei, S. Lin, Z. Xu, Y. Sun, P. Shi, G. Li, L. Bian, Mechanically resilient, injectable, and bioadhesive supramolecular gelatin hydrogels crosslinked by weak host-guest interactions assist cell infiltration and in situ tissue regeneration, Biomaterials 101 (2016) 217–228.
[33] J.Q. Chen, J.B. Yang, L. Wang, X.W. Zhang, B.C. Heng, D.A. Wang, Z.G. Ge, Modified hyaluronic acid hydrogels with chemical groups that facilitate adhesion to host tissues enhance cartilage regeneration, Bioact. Mater. 6 (6) (2021) 1689–1698.
[34] Y.Q. Liang, Z.L. Li, Y. Huang, R. Yu, B.L. Guo, Dual-dynamic-bond cross-linked antibacterial adhesive hydrogel sealants with on-demand removability for post-wound-closure and infected wound healing, ACS Nano 15 (4) (2021) 7078–7093.
[35] A.C. Branco, A.S. Oliveira, I. Monteiro, P. Nolasco, D.C. Silva, C.G. Figueiredo-Pina, R. Colaco, A.P. Serro, PVA-based hydrogels loaded with diclofenac for cartilage replacement, Gels-Basel 8 (3) (2022).
[36] F. Li, A.M. Wang, C.T. Wang, Analysis of friction between articular cartilage and polyvinyl alcohol hydrogel artificial cartilage, J. Mater. Sci. Mater. Med. 27 (5) (2016).
[37] Z.K. Li, D.W. Wang, H.Y. Bai, S.W. Zhang, P.M. Ma, W.F. Dong, Photo-crosslinking strategy constructs adhesive, superabsorbent, and tough PVA-based hydrogel through controlling the balance of cohesion and adhesion, Macromol. Mater. Eng. 305 (1) (2020).
[38] B.S. Kim, I.K. Park, T. Hoshiba, H.L. Jiang, Y.J. Choi, T. Akaike, C.S. Cho, Design of artificial extracellular matrices for tissue engineering, Prog. Polym. Sci. 36 (2) (2011) 238–268.
[39] X.L. Kong, L. Chen, B. Li, C.Y. Quan, J. Wu, Applications of oxidized alginate in regenerative medicine, J. Mater. Chem. B 9 (12) (2021) 2785–2801.
[40] S.L. Levengood, A.E. Erickson, F.C. Chang, M.Q. Zhang, Chitosan-poly (caprolactone) nanofibers for skin repair, J. Mater. Chem. B 5 (9) (2017) 1822–1833.
[41] A.A. Aldana, G.A. Abraham, Current advances in electrospun gelatin-based scaffolds for tissue engineering applications, Int. J. Pharm. 523 (2) (2017) 441–453.
[42] A. Salamon, S. van Vlierberghe, I. van Nieuwenhove, F. Baudisch, G.J. Graulus, V. Benecke, K. Alberti, H.G. Neumann, J. Rychly, J.C. Martins, P. Dubruel, K. Peters, Gelatin-based hydrogels promote chondrogenic differentiation of human adipose tissue-derived mesenchymal stem cells in vitro, Materials 7 (2) (2014) 1342–1359.
[43] G.M. Cunniffe, P.J. Díaz-Payno, E.J. Sheehy, S.E. Critchley, H.V. Almeida, P. Pitacco, S.F. Carroll, O.R. Mahon, A. Dunne, T.J. Levingstone, C.J. Moran, R. T. Brady, F.J. O'Brien, P.A.J. Brama, D.J. Kelly, Tissue-specific extracellular matrix scaffolds for the regeneration of spatially complex musculoskeletal tissues, Biomaterials 188 (2019) 63–73.
[44] E.C. Beck, M. Barragan, T.B. Libeer, S.L. Kieweg, G.L. Converse, R.A. Hopkins, C. J. Berkland, M.S. Detamore, Chondroinduction from naturally derived cartilage matrix: a comparison between devitalized and decellularized cartilage encapsulated in hydrogel pastes, Tissue Eng. 22 (7–8) (2016) 665–679.
[45] T. Novak, B. Seelbinder, C.M. Twitchell, S.L. Voytik-Harbin, C.P. Neu, Dissociated and reconstituted cartilage microparticles in densified collagen induce local hMSC differentiation, Adv. Funct. Mater. 26 (30) (2016) 5427–5436.
[46] Y.B. Basok, A. Kirillova, A. Grigoryev, L. Kirsanova, E. Nemets, V. Sevastianov, Fabrication of microdispersed tissue-specific decellularized matrix from porcine articular cartilage, Inorg. Mater.: Applied Research 11 (5) (2020) 1153–1159.
[47] S. Wakitani, T. Goto, S.J. Pineda, R.G. Young, J.M. Mansour, A.I. Caplan, V. M. Goldberg, Mesenchymal cell-based repair of large, full-thickness defects of articular cartilage, the Journal of bone and joint surgery, Am. Vol. 76 (4) (1994) 579–592.
[48] Y. Han, J. Yang, J. Fang, Y. Zhou, E. Candi, J. Wang, D. Hua, C. Shao, Y. Shi, The secretion profile of mesenchymal stem cells and potential applications in treating human diseases, Signal Transduct. Targeted Ther. 7 (1) (2022) 92.
[49] S. Lecht, C.T. Stabler, A.L. Rylander, R. Chiaverelli, E.S. Schulman, C. Marcinkiewicz, P.I. Lelkes, Enhanced reseeding of decellularized rodent lungs with mouse embryonic stem cells, Biomaterials 35 (10) (2014) 3252–3262.
[50] F.M. Watt, W.T. Huck, Role of the extracellular matrix in regulating stem cell fate, Nat. Rev. Mol. Cell Biol. 14 (8) (2013) 467–473.
[51] S.A. Muhammad, N. Nordin, M.Z. Mehat, S. Fakurazi, Comparative efficacy of stem cells and secretome in articular cartilage regeneration: a systematic review and meta-analysis, Cell Tissue Res. 375 (2) (2019) 329–344.
[52] M.J. Stoddart, J. Bara, M. Alini, Cells and secretome – towards endogenous cell re-activation for cartilage repair, Adv. Drug Deliv. Rev. 84 (2015) 135–145.
[53] B. Balakrishnan, R. Banerjee, Biopolymer-based hydrogels for cartilage tissue engineering, Chem. Rev. 111 (8) (2011) 4453–4474.
[54] L.P. Cao, B. Cao, C.J. Lu, G.W. Wang, L. Yu, J.D. Ding, An injectable hydrogel formed by in situ cross-linking of glycol chitosan and multi-benzaldehyde functionalized PEG analogues for cartilage tissue engineering, J. Mater. Chem. B 3 (7) (2015) 1268–1280.
[55] R. Jin, L.S.M. Teixeira, A. Krouwels, P.J. Dijkstra, C.A. van Blitterswijk, M. Karperien, J. Feijen, Synthesis and characterization of hyaluronic acid-poly (ethylene glycol) hydrogels via Michael addition: an injectable biomaterial for cartilage repair, Acta Biomater. 6 (6) (2010) 1968–1977.
[56] C.A. Vilela, C. Correia, J.M. Oliveira, R.A. Sousa, J. Espregueira-Mendes, R.L. Reis, Cartilage repair using hydrogels: a critical review of in vivo experimental designs, ACS Biomater. Sci. Eng. 1 (9) (2015) 726–739.
[57] J. Li, A.D. Celiz, J. Yang, Q. Yang, I. Wamala, W. Whyte, B.R. Seo, N.V. Vasilyev, J. J. Vlassak, Z. Suo, D.J. Mooney, Tough adhesives for diverse wet surfaces, Science 357 (6349) (2017) 378–381.
[58] W. Wei, Y.Z. Ma, X.D. Yao, W.Y. Zhou, X.Z. Wang, C.L. Li, J.X. Lin, Q.L. He, S. Leptihn, H.W. Ouyang, Advanced hydrogels for the repair of cartilage defects and regeneration, Bioact. Mater. 6 (4) (2021) 998–1011.
[59] Y.L. Yang, J.Y. Zhang, Z.Z. Liu, Q.N. Lin, X.L. Liu, C.Y. Bao, Y. Wang, L.Y. Zhu, Tissue-integratable and biocompatible photogelation by the imine crosslinking reaction, Adv. Mater. 28 (14) (2016) 2724–2730.
[60] H.Y. Wang, S.C. Heilshorn, Adaptable hydrogel networks with reversible linkages for tissue engineering, Adv. Mater. 27 (25) (2015) 3717–3736.

[61] F. Zhou, Y. Hong, X. Zhang, L. Yang, J. Li, D. Jiang, V. Bunpetch, Y. Hu, H. Ouyang, S. Zhang, Tough hydrogel with enhanced tissue integration and in situ forming capability for osteochondral defect repair, Appl. Mater. Today 13 (2018) 32–44.
[62] A. Cholewinski, F. Yang, B.X. Zhao, Algae-mussel-inspired hydrogel composite glue for underwater bonding, Mater. Horiz. 6 (2) (2019) 285–293.
[63] S. Liang, Y.Y. Zhang, H.B. Wang, Z.Y. Xu, J.R. Chen, R. Bao, B.Y. Tan, Y.L. Cui, G. W. Fan, W.X. Wang, W. Wang, W.G. Liu, Paintable and rapidly bondable conductive hydrogels as therapeutic cardiac patches, Adv. Mater. 30 (23) (2018).
[64] X.W. Liu, H.J. Yu, L. Wang, Z.K. Huang, F. Haq, L.S. Teng, M.J. Jin, B.B. Ding, Recent advances on designs and applications of hydrogel adhesives, Adv. Mater. Interfac. 9 (2) (2022).
[65] P. Heidarian, A.Z. Kouzani, A. Kaynak, B. Bahrami, M. Paulino, B. Nasri-Nasrabadi, R.J. Varley, Rational design of mussel-inspired hydrogels with dynamic catecholato-metal coordination bonds, Macromol. Rapid Commun. 41 (23) (2020).
[66] Y.X. Mao, P. Li, J.W. Yin, Y.J. Bai, H. Zhou, X. Lin, H.L. Yang, L. Yang, Starch-based adhesive hydrogel with gel-point viscoelastic behavior and its application in wound sealing and hemostasis, J. Mater. Sci. Technol. 63 (2021) 228–235.
[67] Y. Qin, C. Qiu, Y. Hu, S.J. Ge, J.P. Wang, Z.Y. Jin, In situ self-assembly of nanoparticles into waxberry-like starch microspheres enhanced the mechanical strength, fatigue resistance, and adhesiveness of hydrogels, ACS Appl. Mater. Interfaces 12 (41) (2020) 46609–46620.
[68] W. Wang, Y.Y. Zhang, W.G. Liu, Bioinspired fabrication of high strength hydrogels from non-covalent interactions, Prog. Polym. Sci. 71 (2017) 1–25.
[69] D.J. Laird, U.H. von Andrian, A.J. Wagers, Stem cell trafficking in tissue development, growth, and disease, Cell 132 (4) (2008) 612–630.
[70] S. Pacelli, S. Basu, J. Whitlow, A. Chakravarti, F. Acosta, A. Varshney, S. Modaresi, C. Berkland, A. Paul, Strategies to develop endogenous stem cell-recruiting bioactive materials for tissue repair and regeneration, Adv. Drug Deliv. Rev. 120 (2017) 50–70.
[71] R.M. Frank, E.J. Cotter, I. Nassar, B. Cole, Failure of bone marrow stimulation techniques, Sports Med. Arthrosc. Rev. 25 (1) (2017) 2–9.
[72] D.J. Mooney, H. Vandenburgh, Cell delivery mechanisms for tissue repair, Cell Stem Cell 2 (3) (2008) 205–213.
[73] E.L. Fong, C.K. Chan, S.B. Goodman, Stem cell homing in musculoskeletal injury, Biomaterials 32 (2) (2011) 395–409.
[74] Z. Tang, Y. Lu, S. Zhang, J. Wang, Q. Wang, Y. Xiao, X. Zhang, Chondrocyte secretome enriched microparticles encapsulated with the chondrocyte membrane to facilitate the chondrogenesis of BMSCs and reduce hypertrophy, J. Mater. Chem. B 9 (48) (2021) 9989–10002.
[75] J. Shin, J.S. Lee, C. Lee, H.J. Park, K. Yang, Y. Jin, J.H. Ryu, K.S. Hong, S.H. Moon, H.M. Chung, H.S. Yang, S.H. Um, J.W. Oh, D.I. Kim, H. Lee, S.W. Cho, Tissue adhesive catechol-modified hyaluronic acid hydrogel for effective, minimally invasive cell therapy, Adv. Funct. Mater. 25 (25) (2015) 3814–3824.
[76] X.Y. Xu, X.F. Xia, K.Y. Zhang, A. Rai, Z. Li, P.C. Zhao, K.C. Wei, L. Zou, B.G. Yang, W.K. Wong, P.W.Y. Chiu, L.M. Bian, Bioadhesive hydrogels demonstrating pH-independent and ultrafast gelation promote gastric ulcer healing in pigs, Sci. Transl. Med. 12 (558) (2020).
[77] X. Peng, X.F. Xia, X.Y. Xu, X.F. Yang, B.G. Yang, P.C. Zhao, W.H. Yuan, P.W. Y. Chiu, L.M. Bian, Ultrafast self-gelling powder mediates robust wet adhesion to promote healing of gastrointestinal perforations, Sci. Adv. 7 (23) (2021).
[78] S. Reakasame, A.R. Boccaccini, Oxidized alginate-based hydrogels for tissue engineering applications: a review, Biomacromolecules 19 (1) (2018) 3–21.
[79] M. Friedman, Applications of the ninhydrin reaction for analysis of amino acids, peptides, and proteins to agricultural and biomedical sciences, J. Agric. Food Chem. 52 (2004) 385–406.
[80] B.D. Elder, S.V. Eleswarapu, K.A. Athanasiou, Extraction techniques for the decellularization of tissue engineered articular cartilage constructs, Biomaterials 30 (22) (2009) 3749–3756.
[81] Q. Yang, J. Peng, Q. Guo, J. Huang, L. Zhang, J. Yao, F. Yang, S. Wang, W. Xu, A. Wang, A cartilage ECM-derived 3-D porous acellular matrix scaffold for in vivo cartilage tissue engineering with PKH26-labeled chondrogenic bone marrow-derived mesenchymal stem cells, Biomaterials 29 (15) (2008) 2378–2387.
[82] B. Wen, R. Zhou, Q. Feng, Q. Wang, J. Wang, S. Liu, IQuant: an automated pipeline for quantitative proteomics based upon isobaric tags, Proteomics 14 (20) (2014) 2280–2285.
[83] L. Feng, Z. Yang, Y. Li, Q. Pan, X. Zhang, X. Wu, J.H.T. Lo, H. Wang, S. Bai, X. Lu, M. Wang, S. Lin, X. Pan, G. Li, MicroRNA-378 contributes to osteoarthritis by regulating chondrocyte autophagy and bone marrow mesenchymal stem cell chondrogenesis, Mol. Ther. Nucleic Acids 28 (2022) 328–341.
[84] M. Wang, Y. Li, L. Feng, X. Zhang, H. Wang, N. Zhang, I. Viohl, G. Li, Pulsed electromagnetic field enhances healing of a meniscal tear and mitigates posttraumatic osteoarthritis in a rat model, Am. J. Sports Med. 50 (10) (2022) 2722–2732.
[85] R.L. Dahlin, L.A. Kinard, J. Lam, C.J. Needham, S. Lu, F.K. Kasper, A.G. Mikos, Articular chondrocytes and mesenchymal stem cells seeded on biodegradable scaffolds for the repair of cartilage in a rat osteochondral defect model, Biomaterials 35 (26) (2014) 7460–7469.
[86] Y. Li, Q. Pan, N. Zhang, B. Wang, Z. Yang, J.T. Ryaby, E.I. Waldorff, W.Y.-W. Lee, G. Li, A novel pulsed electromagnetic field promotes distraction osteogenesis via enhancing osteogenesis and angiogenesis in a rat model, Journal of Orthopaedic Translation 25 (2020) 87–95.